SACLANTCEN REPORT
serial no.: SR-154

SACLANT UNDERSEA
RESEARCH CENTRE

REPORT

Optimum bearing resolution for a moving towed array and extension of its physical aperture

S. Stergiopoulos

April 1989

Page count for SR-154
(excluding covers)

Pages	Total
i–vi	6
1–45	45
	51

SACLANT Undersea Research Centre
Viale San Bartolomeo 400
19026 San Bartolomeo (SP), Italy

tel: 0187 540 111
telex: 271148 SACENT I

NORTH ATLANTIC TREATY ORGANIZATION

SACLANTCEN SR-154

Optimum bearing resolution for a moving towed array and extension of its physical aperture

S. Stergiopoulos

The content of this document pertains to work performed under Project 02 of the SACLANTCEN Programme of Work. The document has been approved for release by The Director, SACLANTCEN.

Peter C. Wille
Director

intentionally blank page

SACLANTCEN SR-154

Optimum bearing resolution for a moving towed array and extension of its physical aperture

S. Stergiopoulos

Executive Summary: A continuing goal in sonar systems is to increase the detection range. As a result, towed arrays have been introduced in operational sonar systems, which has made the listening frequency range lower to achieve attenuation. Since the low-frequency regime includes mainly traffic noise, high bearing resolution is required for the angular separation of closely spaced ships. Because the increased low-frequency bearing resolution means longer hydrophone arrays with consequent technical and operational implications, many attempts have been made to increase effective array length by synthesizing additional hydrophones. These efforts have included the application of the so-called 'synthetic aperture techniques', which have been successfully used in aircraft and satellite active radar systems. But, because of the presence of disturbed motion of the array by currents, such applications have not been successful for cases of passive sonars.

The present investigation deals with the fundamental problems of improving bearing resolution of a moving array from both theoretical and experimental points of view. The angular resolution capability of a towed array is investigated by including the movement of the array in theoretical models. In the experimental phase an extended towed-array algorithm is introduced into this problem. The performance of this algorithm for extending the physical aperture of an array agrees with the theoretical bounds for values of signal-to-noise ratio higher than -8 dB *re* 1 Hz band at the hydrophone level.

Real data applications of the extended towed-array algorithm were successful and the physical aperture of a 32-hydrophone towed array was extended to an equivalent of a 512-hydrophone fully populated array. The robustness of the above algorithm was demonstrated with experimental data having very low signal-to-noise ratio broadband signal and for a pure tone even though the source had 3.6 kn speed along its bearing. These experimental results indicate that the coherence in the underwater environment can be sufficient to extend the physical aperture of a conventional towed array by more than one order of magnitude. To define, however, the optimum extended aperture of a towed array, further studies are necessary to adapt the parameters of this algorithm into a real operational environment where many ships and targets with vey low levels of radiated noise will be considered.

intentionally blank page

SACLANTCEN SR-154

Optimum bearing resolution for a moving towed array and extension of its physical aperture

S. Stergiopoulos

Abstract: This report examines the limits of the angular resolution capability of a moving towed array (MTA) by finding the Cramer–Rao lower bound (CRLB), provides algorithms that extend the physical aperture of an MTA and compares the performance of these algorithms with the limits provided by the CRLBs.

The model which is considered for the CRLB estimates assumes that an N hydrophone towed array is moving with known constant speed and that in the received signal unknowns are all the parameters (i.e. amplitude, frequency, bearing, initial phase) for two sources. The estimated CRLBs for this model indicated that an N-hydrophone MTA provides very high angular resolution when the duration T of the received signal is very long. This ability of the moving array to resolve two closely spaced sources is related to the fact that the physical aperture has been extended by the distance travelled by the array during the T seconds of the observation period. In the case of one source, the MTA has improved performance in comparison with a stationary array under the assumption that the transmitted frequency of the source is known.

Computer simulation examples using a maximum likelihood estimator and an extended towed-array algorithm to find the bearings of sources are presented. The results of these simulations agree with the CRLB if the signal-to-noise ratio is higher than 0 dB at the hydrophone level. Below this value the performance of both methods rapidly deteriorates.

Applications of the extended towed-array algorithm on real data were successful, and the physical aperture of a 32-hydrophone MTA was extended to an equivalent of a 512-hydrophone fully populated stationary array.

Keywords: coherence ○ conventional beamformer ○ Cramer–Rao lower bound ○ extended towed-array measurements ○ maximum likelihood estimator ○ overlapped correlator ○ synthetic aperture ○ variance of estimates

Contents

Acknowledgement: The author would like to express his appreciation to A.H. Nuttall of NUSC for his valuable comments and discussions, to P.J. Enoch and the members of his LRG group for providing the experimental data and J.P. Ianniello for his valuable comments about the CRLBs.

1 Introduction

A continuing goal in towed-array research is the improvement of bearing resolution. Many efforts have been made in this area of research. The related techniques for improving the angular resolution of a receiving array, the so-called 'synthetic aperture' techniques, use mainly the fact that the array is moving. While these techniques have been successfully applied to aircraft and satellite active radar systems, they have not been successful with sonar systems, because of the presence of disturbed paths of the towed array and the poor coherence of the acoustic signal in the sea as compared to the electromagnetic waves in the air.

Recent experimental studies [1–3], however, have indicated that the space and time coherence of the acoustic signal in the sea appears to be sufficient to extend the physical aperture of a moving towed array (MTA). It has been also suggested by several numerical studies [4–6] that the improved prospects for extending successfully the physical aperture of a towed array require algorithms which are not based on the synthetic aperture concept used in active radars. In one of these works the author of this report and Sullivan [5] introduced an algorithm for extended towed-array measurements (ETAM) that achieves a desired aperture size using an N-hydrophone MTA. The basic idea in this algorithm is a phase correction factor that is used to combine successive measurements of the MTA coherently to extend the effective towed-array length. The decisive phase correction factor is derived by cross-correlating successive hydrophone signals of the array that overlap. Because of the spatial overlapping, the algorithm properly compensates for the phase fluctuations of the received signal caused by irregularities of the tow path of the physical array and the acoustic propagation characteristics. As a result it is not necessary to have accurate estimates of the source frequency or a manoeuvre in order to obtain a wavenumber or bearing estimate as is required by the standard passive synthetic aperture technique.

Applications of the above algorithm to real data, for improvement of the angular resolution of an array by extending its physical aperture, were successful and the results are reported here. As expected, applications of the synthetic aperture technique on the same set of real data provided very poor results. Consequently questions were raised about the performance of the ETAM algorithm for data having very low signal-to-noise ratio (SNR), and about the best estimation that can be made with the available data. Statistics suggest that the Cramer–Rao lower bound (CRLB) [7–9] provides the minimum variance achievable by any unbiased estimator.

The angular resolution capability of a MTA and the amount of information inherent in a received signal can also be investigated by the use of the CRLB or information inequality.

This report deals with these questions and problems as follows. In Sect. 2 the CRLB estimates are derived for a model which assumes that an N-hydrophone towed array is moving with known constant speed, and in the T seconds of received signal, all the parameters (i.e. amplitude, frequency, bearing, initial phase) for two sources are unknown. Other cases are also examined by having one source and some of the above parameters known. In this way, the lack of knowledge for these parameters is investigated.

If there exists a signal processor to achieve the CRLB, it will be the maximum likelihood estimation (MLE) technique. The MLE asymptotically reaches the CRLB, but below a threshold SNR, its performance suddenly deteriorates. This threshold effect has been established for similar problems in many studies [10,11]. In Sect. 3, computer simulation examples are presented using the MLE and the ETAM to estimate bearings. The results from these simulations are compared with the CRLB which is used as a standard of performance, and the threshold SNR for both techniques is established. The MLE used in this work has been developed by Nuttall [12] and, since it has not been published yet, it is discussed briefly in Sect. 3.

The applications of the MLE and the ETAM to real data are included in Sect. 4. The available space and time coherence in the sea is discussed in Sect. 5, based on the experimental results for extending the physical aperture of the MTA. In the same section, recommendations are made for additional work necessary in order to examine and exploit the merits of the ETAM and the MLE for specific applications.

2 Theory

Let us consider the following model. Two sources continuously radiate pure tones as acoustic signals. A linear towed array, which is assumed to be at a very large distance from these sources and moving with constant speed V_T along a straight-line course, receives these acoustic signals as incident plane waves. The array has N equally spaced hydrophones, with d being their spacing. The received signal at the nth hydrophone is

$$y_n(\Theta, t_i) = \sum_{k=1}^{2} A_k \cos\left[\omega_k\left(t_i + \frac{d(n-1)}{C}\cos\beta_k\right) + \Phi_k\right] + \epsilon_{n,i}(0, \sigma_N). \qquad (1)$$

In the above equation $\omega_k = \Omega_k\,(1 - (V_k - V_T\,\cos\beta_k)/C)$ is the received frequency which is defined to include the doppler shift, Ω_k the frequency of the stationary field, A_k the amplitude, V_k the speed along the β_k bearing of the kth source and C the propagation speed for the plane waves.

The acoustic signal is sampled at time increment Δt with $t_i = i\Delta t$, where $i = 1, 2, \ldots, M$ (M being the number of data points for each hydrophone time series). $\epsilon_{n,i}(0, \sigma_N)$ are independent, zero mean, gaussian random variables with variance σ_N^2. The vector Θ includes all the unknown parameters considered in Eq. (1).

Let $\sigma_{\theta_i}^2$ denote the variance of an unbiased estimate of an unknown parameter θ_i in the vector Θ. The Cramer–Rao [13] bound states that the best unbiased estimate $\tilde{\Theta}$ of the parameter vector Θ has the covariance matrix

$$\mathrm{cov}\tilde{\Theta} \geq J(\Theta)^{-1}, \qquad (2)$$

where J is the Fisher information matrix whose elements are

$$J_{ij} = -E\left[\frac{\partial^2 \ln P(Y|\Theta)}{\partial\theta_i \partial\theta_j}\right], \qquad (3)$$

$E[\ldots]$ denotes the expectation operator and $P(Y|\Theta)$ is the probability density governing the observations $Y = [y_1(t_i), y_2(t_i), \ldots, y_N(t_i)]$, where $i = 1, 2, \ldots, M$ for M independent time samples for each of the N independent space samples which are described by the model in Eq. (1).

The variance $\sigma^2_{\theta_i}$ of the unbiased estimates $\tilde{\Theta}$ has a lower bound (called the CRLB) which is given by the diagonal elements of Eq. (2). This CRLB is used as the standard of performance and provides a good measure for the performance of a signal processing algorithm which gives unbiased estimates $\tilde{\Theta}$ for parameter vector Θ.

In this report we assume that the component of the velocity along the bearing for each source is negligible, or $V_k = 0$, and that the speed V_T of the array is known. Then the unknown parameters in the vector Θ are $\Theta = (A_k, \Omega_k, \beta_k, \Phi_k)^T$, $k = 1, 2$ according to model (1).

The simplest problem of one source with the bearing β_1 being the unknown parameter and for a stationary array $V_T = 0$ has been discussed [14] and following Eq. (3), the results of the variance $\sigma^2_{\beta_1}$ in the bearing measurements are

$$\sigma^2_{\beta_1} = \frac{3}{2RN} \left(\frac{B_w}{\pi \sin \beta_1} \right)^2, \tag{4}$$

where N is considered to be large, $R = MA_1^2/\sigma_N^2$ and the SNR at the hydrophone is $\text{SNR} = 10 \log_{10}(R)$. The parameter $B_w = \lambda/(N-1)d$ gives the beamwidth of the physical aperture of the array and λ is the wavelength corresponding to ω_k.

Consider now the case of a moving array ($V_T \neq 0$) for the same problem as above. Then the results of the variance $\sigma^2_{\beta_1}(V_T)$ are derived in the same way as before and are

$$\sigma^2_{\beta_1}(V_T) = \frac{\sigma^2_{\beta_1}}{1 + (3/2)((V_T T/\lambda)B_w) + ((V_T T/\lambda)B_w)^2 - (3/8\pi^2)((V_T/C)B_w)^2}, \tag{5}$$

where, for simplicity, a broadside source ($\beta_1 \simeq \frac{1}{2}\pi$) is taken. It is obvious from the above expression that the variance of the bearing, $\sigma^2_{\beta_1}(V_T)$, gets smaller for a moving rather than a stationary array when the observation period T becomes long.

For the following cases we are going to examine, the elements of the Fisher information matrix in Eq. (3) include in their analytical derivations double summations over time and space, and their expressions are too long to be presented here. These analytical derivations are shown in Appendix A and are consistent with the numerical estimates of the elements of the above matrix.

We have chosen to use the σ^2_β ($V_T = 0$) as the normalized parameter for the estimates of $\sigma^2_\beta(V_T)$ for all the different cases considered in this report. In this way, any improvement or possible exploitation of the amount of information inherent in a moving array (in comparison with a stationary one) can be investigated. This investigation is divided here into two main parts: (1) the problem of one source and (2) the problem of two sources.

2.1. ONE SOURCE

In Fig. 1 the dependence of the CRLB estimates for the variance $\sigma^2_{\beta_1}(V_T)$, which is normalized by $\sigma^2_{\beta_1}$ $(V_T = 0)$, is shown as a function of the observation period. When (β_1) or (A_1, β_1) are considered as the unknowns in the parameter vector Θ, the curve 1 in this figure gives the dependence of the normalized $\sigma^2_{\beta_1}(V_T)$ on the observation period for a moving array.

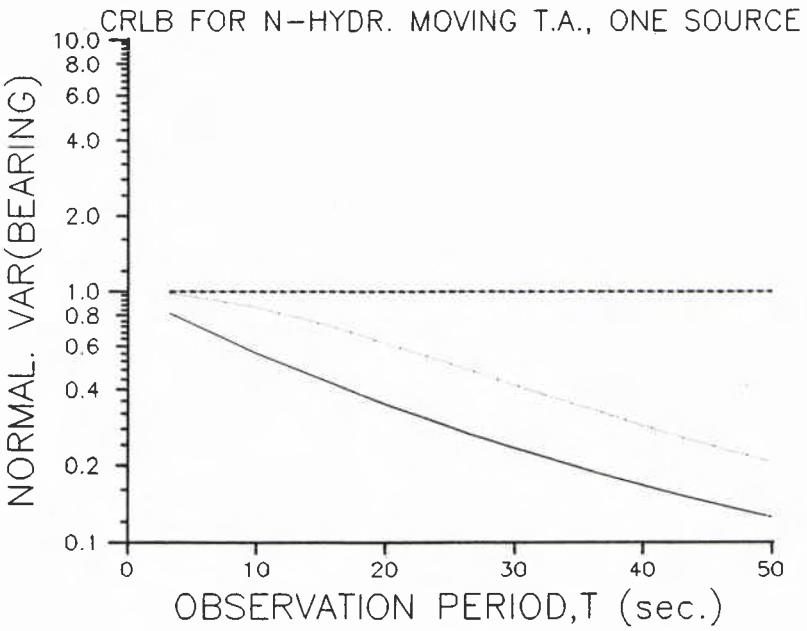

Fig. 1. The dependence of the CRLB estimates for the variance of bearing $\sigma^2_{\beta_1}(V_T)$ for a moving towed array as a function of the observation period. These CRLB estimates have been normalized by the results of $\sigma^2_{\beta_1}(V_T = 0)$ for a stationary array and refer to the case when one source is known to exist. Curve 1 (solid line) gives the normalized variance of the bearing when β_1 or (A_1, β_1) are the unknown parameters. Curve 2 (dotted line) gives the normalized variance for bearing when (A_1, β_1, Φ_1) are the unknown parameters. Curve 3 (dashed line) gives the variance of bearing when unknown parameters are $(A_1, \Omega_1, \beta_1, \Phi_1)$.

The results of this figure clearly indicate the improvement in bearing estimates with a moving array and for long observation periods in comparison with a stationary one. In the case that (A_1, β_1, Φ_1) are the unknowns in the vector Θ we see, from curve 2 in this figure, the improved estimates for β_1 provided by an MTA in comparison

with the ones given by a stationary array. These estimates, however, are inferior to the results in curve 1. In all the above cases, the speed of the MTA was chosen to be 5 kn (i.e. 2.5 m/s).

When $(A_1, \Omega_1, \beta_1, \Phi_1)$ are the unknowns in the vector Θ, we clearly see by the results of curve 3 in the same Fig. 1 that there is no improvement in the estimates of β_1 when a moving or a stationary array is used. In other words, as the lack of knowledge of the parameters of the one source increases, then there is a corresponding loss in the performance of an unbiased estimator trying to exploit the amount of information inherent in a moving array in comparison with a stationary one. As expected, when the frequency Ω_1 and the bearing β_1 are the unknown parameters associated with the problem of one source, then there is no gain or better performance using a moving or stationary array for bearing estimates, since in a passive towed-array system, the doppler shift cannot be determined. It is the doppler shift in the model (1) which exploits the amount of information provided by a moving array.

Since the lack of knowledge of the parameters $(A_1, \Omega_1, \beta_1, \Phi_1)$ on the estimates of the bearing β_1 has been established by the results of Fig. 1 we can continue now to examine the effects of the speed of the moving array and the bearing of the source on the variance $\sigma^2_{\beta_1}(V_T)$ by having the parameters $(A_1, \Omega_1, \beta_1, \Phi_1)$ unknown. In Fig. 2, we have the dependence of the variance $\sigma^2_{\beta_1}(V_T)$ on the speed of the MTA. The curve 1 in this figure indicates that the speed of the towed array does not have any influence on the $\sigma^2_{\beta_1}(V_T)$, which is normalized by $\sigma^2_{\beta_1}$ $(\beta_1 = \pi/2,\ V_T = 0)$, for different values of the observation period and for the source being at broadside. When the source has bearing $\beta_1 = 45°$ we see by the results of curve 2 that the variance $\sigma^2_{\beta_1}(V_T)$, which is normalized by $\sigma^2_{\beta_1}$ $(\beta_1 = \pi/4,\ V_T = 0)$, increases linearly with the speed of the MTA. This increase, however, is very small, and for the speed of the MTA being 5 kn, the increase in $\sigma^2_{\beta_1}(V_T)$ is 0.2% and independent of the observation period.

Presented in Fig. 3 is the dependence of the variance of the frequency $\sigma^2_{\Omega_1}(V_T)$ on the speed of the MTA and for different observation periods. The parameter $\sigma^2_{\Omega_1}(V_T)$ has been normalized by $\sigma^2_{\Omega_1}$ $(V_T = 0)$. It is clearly seen by the results of this figure that the performance of an unbiased estimator for the estimates of the frequency Ω_1 deteriorates as the speed of the MTA increases and this deterioration in performance is more evident when the observation period gets longer.

The results in Figs. 2 and 3 are consistent with the ones of curve 3 in Fig. 1. In other words the frequency Ω_1 in all the above cases has been considered as an unknown parameter and the doppler shift, which provides the additional information in an MTA in comparison with the stationary one, can not be determined by a passive array. Thus, the movement of the array does not provide any improvement in the bearing estimates for the problem of the one source when the frequency Ω_1 is unknown. In fact when the source is not at broadside, this movement is the cause of

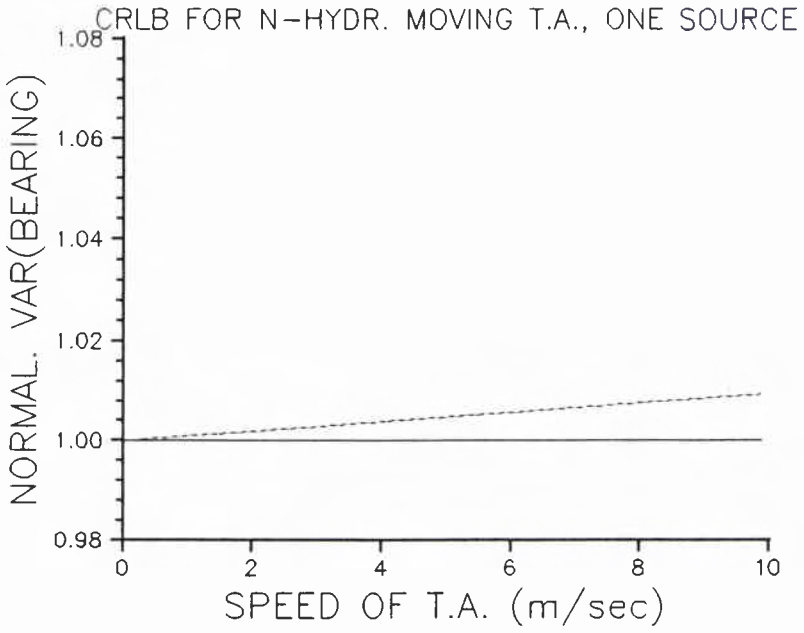

Fig. 2. The dependence of the variance of bearing $\sigma^2_{\beta_1}(V_T)$ on the speed of a moving towed array for the case when one source is known to exist and unknowns are all the parameters (A_1, Ω_1, β_1, Φ_1). The above CRLB estimates have been normalized by the equivalent estimates $\sigma^2_{\beta_1}(V_T = 0)$ for a stationary array. Curve 1 (solid line) gives the dependence of the normalized variance of the bearing on the speed of the MTA when the source is broadside to the receiving array and for different observation periods (T = 1.0, 10 s). Curve 2 (dashed line) gives the normalized variance for bearing as a function of the speed of the MTA when the source has 45° bearing and for different observation periods (T = 1.0, 10 s).

a slight deterioration of the bearing estimates using an MTA instead of a stationary array, as is shown by curve 2 in Fig. 2.

In order to reinforce the above point, we have carried out the calculations presented in Fig. 2 for the case that the (A_1, β_1, Φ_1) are the unknown parameters. The results in this case are given in Fig. 4 where the source has bearing $\beta_1 = 45°$. The curve 1 in this figure shows that the $\sigma^2_{\beta_1}$ ($\beta_1 = \pi/4$, V_T, $T = 0.1$ s), which is normalized by $\sigma^2_{\beta_1}$ ($\beta_1 = \pi/4$, $V_T = 0$, $T = 0.1$ s), does not depend on the speed of the MTA as in curve 2 of Fig. 2. One should expect, therefore, that the estimates of $\sigma^2_{\beta_1}(V_T)$ in curve 1 of Fig. 4 should be better for longer observation periods. This expectation is correct and it is shown by the results of curve 2 in Fig. 4 where $\sigma^2_{\beta_1}$ ($\beta_1 = \pi/4$,

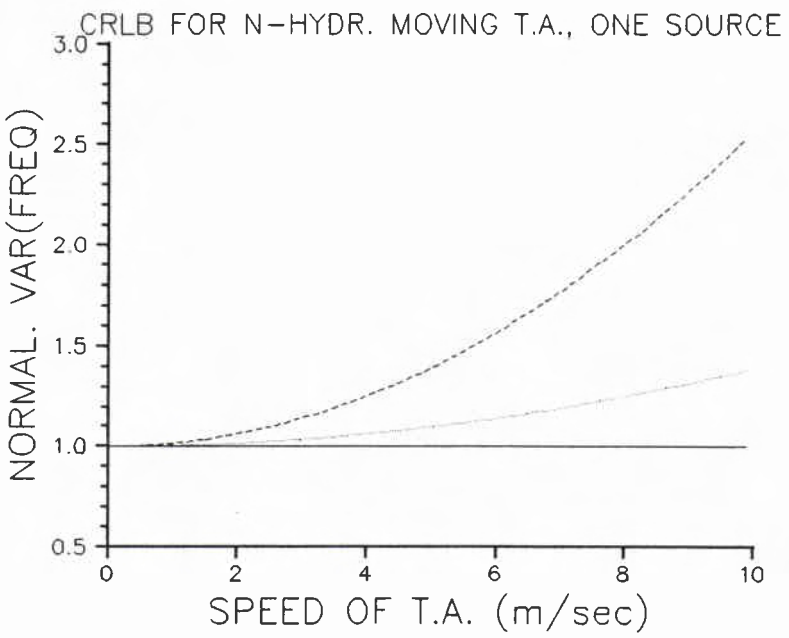

Fig. 3. The dependence of the variance of frequency $\sigma^2_{\Omega_1}(V_T)$ on the speed of a moving towed array for the case when one source is known to exist and unknowns are all the parameters (A_1, Ω_1, β_1, Φ_1). The above CRLB estimates have been normalized by the equivalent estimates $\sigma^2_{\Omega_1}(V_T = 0)$ for a stationary array. Curve 1 (solid line) gives the dependence of the normalized variance of the frequency on the speed of the MTA when the source has 45° bearing and the observation period is $T = 1.0$ s. Curve 2 (dotted line) is for $T = 5$ s. Curve 3 (dashed line) is for $T = 10$ s.

V_T, $T = 10$ s), which is normalized by $\sigma^2_{\beta_1}$ ($\beta_1 = \pi/4$, $V_T = 0$, $T = 10$ s), decreases as the MTA moves faster.

2.2. TWO SOURCES

For the case when there are two sources ($k = 2$), the unknown parameters in the vector Θ are considered to be (A_k, Ω_k, β_k, Φ_k), $k = 1, 2$. Presented in Fig. 5 are the estimates of $\sigma^2_{\beta_{k=1,2}}(V_T)$, which are normalized by $\sigma^2_{\beta_0}$ given by Eq. (4). The frequencies of the two sources are considered to be very close ($\mid \Omega_1 - \Omega_2 \mid \leq 2\pi/10T$). Curve 1 of this figure shows the normalized estimates of $\sigma^2_{\beta_{k=1,2}}$ (V_T, $T = 1$ s) for a very short observation period. The results of this curve exhibit a behaviour almost identical to those of a stationary array [8,9], which is shown here by curve 2. This

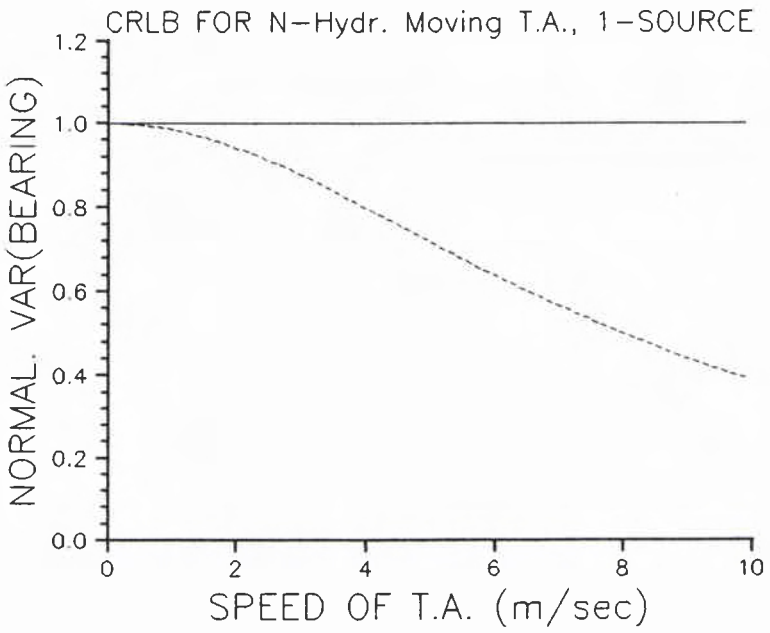

Fig. 4. The dependence of the variance of bearing $\sigma^2_{\beta_1}(V_T)$ on the speed of a moving towed array for the case when one source is known to exist and unknowns are the parameters (A_1, β_1, Φ_1). The above CRLB estimates have been normalized by the equivalent estimates $\sigma^2_{\beta_1}(V_T = 0)$ for a stationary array. Curve 1 (solid line) gives the dependence of the normalized variance of the bearing on the speed of the MTA when the source has 45° bearing and for $T = 0.1$ s observation period. Curve 2 (dashed line) gives the dependence of the normalized variance of the bearing on the speed of the MTA when the source has 45° bearing and for $T = 10$ s observation period.

behaviour states that as the target separation becomes less than the beamwidth of the array, the resolution capability of the array deteriorates rapidly.

When the case of a very long observation period ($T \simeq 180$ s) is considered, the results of the normalized variance $\sigma^2_{\beta_{k=1,2}}$ $(V_T, T = 180$ s) are given by curve 3 of Fig. 5. These results indicate very clearly that in this case, the MTA has better ability than before to resolve two closely spaced sources. This ability is related to the fact that the physical aperture has been extended by the distance travelled by the MTA during the T seconds of the observation period. As expected, the above estimates of $\sigma^2_{\beta_{k=1,2}}(V_T)$ are improved when the frequencies ω_k $(k = 1, 2)$ are assumed known.

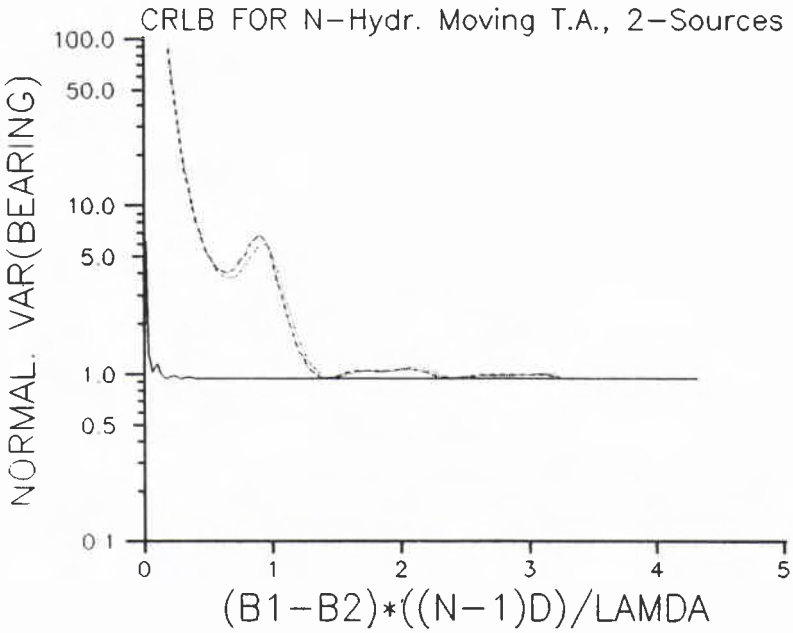

Fig. 5. CRLB estimates of the variance of bearing $\sigma^2_{\beta_{k=1,2}}(V_T)$ as a function of the angular separation of the two sources, which are known to exist. Unknowns are all the parameters $(A_k, \Omega_k, \beta_k, \Phi_k)$, $k = 1, 2$. The above CRLB estimates have been normalized by $\sigma^2_{\beta_1}$ for a stationary array given by Eq. (4). The angular separation of the two sources has been normalized by $B_w = \lambda/(N-1)d$, which is the beamwidth of the physical aperture of the receiving array having $N = 32$ hydrophones with $d = 0.98$ m spacing. Curve 1 (dashed line) gives the angular resolution capability of the MTA for a very short observation period $T = 1.0$ s. The results in curve 1 are nearly identical with those of a stationary towed array shown here by curve 2 (dotted line). Curve 3 (solid line) gives the angular resolution capability of the MTA for a very long observation period $T = 180$ s.

If the results are compared between those of the one-source case with the results of the two-source case, the following main conclusion is made. When the frequency and the bearing of sources are unknown, the amount of information inherent in an MTA is provided as extended angular resolution which is proportional to the observation period. In the case when only one source is known to exist, the MTA has improved performance for bearing estimates in comparison with a stationary array only when the frequency of the source is known.

3

Estimators and threshold effect

Following the investigation by the use of the CRLB of the amount of information that could be available by an MTA, the next question needed to be addressed here is about the unbiased estimators which can exploit this available information and provide results asymptotically reaching the CRLBs. The estimators which may reach the above goal are proposed in this report and are the ETAM algorithm developed by Stergiopoulos and Sullivan [5] and an MLE technique introduced by Nuttall [12]. A brief description of these estimators follows.

3.1. ETAM ALGORITHM

The physical concept of the algorithm for extended towed-array measurements (ETAM) has been discussed in Sect. 1. The processor design of this concept is illustrated in Fig. 6. The key parameters in the ETAM method are the following: $\tau = qd/V_T$ is the time increment between two successive sets of measurements, q represents the number of hydrophone positions that the towed array has moved during the τ seconds or the number of hydrophones the physical aperture of the MTA is extended at each successive set of measurements, and J is the total number of sets of measurements required to achieve a desired extended aperture size. Thus the integration period of the extended towed-array processing is $T = J\tau$.

Between two successive set of measurements $(l, l+1)$ there are $N-q$ pairs of space samples and each one of them represents the same position in space. These $N-q$ pairs of space samples provide the phase correction factor $\tilde{\Psi}(\omega_m, \tau)$ of the ETAM which coherently combines the successive space measurements by an MTA in order to extend the physical aperture. The $\tilde{\Psi}(\omega_m, \tau)$ is defined by

$$\tilde{\Psi}(\omega_m, \tau) = \arg\left[\frac{1}{N-q}\sum_{y=1}^{N-q}[Y_{l,n_0}(\omega_m)|Y^{\dagger}_{(l+1),n}(\omega_m)]_y\right], \tag{6}$$

where $\dagger$ denotes complex conjugate of the $Y_{l,n}(\omega_m)$ space sample of the hydrophone time series in the frequency domain at a frequency ω_m of interest. $n_0 = q+1, q+2, \ldots, N$ are the hydrophones of the lth set of measurements and $n = 1, 2, \ldots, N-q$ are the hydrophones of the next $(l+1)$ set of measurements, which have the same position in space with those of the lth set.

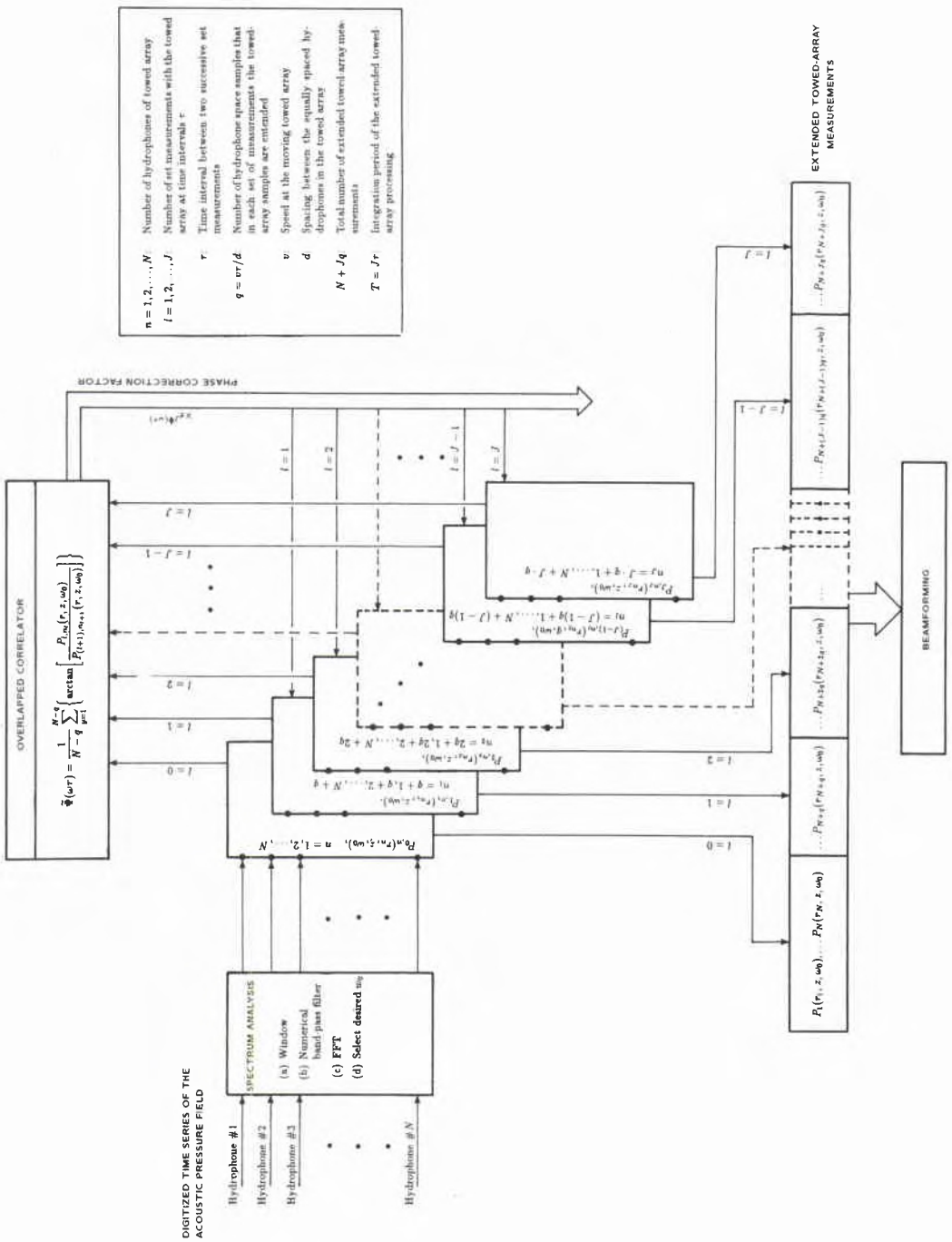

Fig. 6. Schematic of the processor design regarding the extended towed-array processing by overlapped correlator.

At this point it should be mentioned that a beamforming technique is neccessary in order to derive the bearing estimates from the extended towed-array measurements using the ETAM algorithm. In a previous study [5] the performance of the well-known beamforming techniques on the extended towed-array samples was examined. The conclusion from this examination was that the conventional beamformer (CBF) without shading is the optimum beamformer to recover the bearing spectrum from the ETAM. The CBF is defined by $S_{\mathrm{CBF}}(\beta) = d_n^{\dagger}(\beta) R_{YY} d_n(\beta)$, where $d_n(\beta) = \exp[i\omega/Cd(n-1)\cos\beta]$ is the direction vector and R_{YY} the cross-correlation matrix of the space samples $Y_n(\omega)$. In this study the CBF is the beamformer which is used to recover the bearing spectrum from the ETAM.

When idealized parameters are assumed, the expected value of the phase correction factor in Eq. (6) is $\tilde{\Psi}(\omega_m, \tau) = \omega_m \tau$, where τ is known and ω_m is derived from the power spectrum of the hydrophone time series. This idealized expression for the phase correction factor is used in the conventional synthetic aperture technique [15] to extend the physical aperture of an array. When reference is made in this report to the synthetic aperture technique, the above idealized expression for the phase correction factor is assumed.

The effects on the ETAM algorithm of the towed-array placement errors, the coherence of the media, and the frequency variations of the signal have been examined [5]. The SNR at the hydrophone for the ETAM during the T seconds, which are required to extend the physical aperture of an MTA to a desired size, is defined by

$$\mathrm{SNR}_{\mathrm{ETAM}} = 20\log_{10}(A/\sigma_N) + 10\log_{10}(M) + 5\log_{10}(J+1). \tag{7}$$

Equation (7) indicates that there are $(J+1)$ times M number of data points for each of the hydrophone time series which are processed during the T seconds of the observation period.

3.2. MLE

If there exists a signal processor to achieve the CRLB it will be the maximum likelihood estimation (MLE). Nuttall [12] has studied this problem of the MTA and even though his work is not complete yet, some of his results apply directly in the present study. We will discuss these results since they are not yet available.

The approach followed in the above study includes an X-Y coordinate system where the general positions of a moving source and an N-hydrophone moving array are defined. The notation used here and the definition of the related parameters is the same as in Sect. 2. At time t_1 an impulse is emitted by a source located at $\tilde{r}_s(t) = [(r_{x_s} + V_{x_s}t), (r_{y_s} + V_{y_s}t)]^{\tau}$ and the velocity vector of this source is $\tilde{V}_s = [V_{x_s}, V_{y_s}]^{\tau}$. This signal is received by the nth hydrophone of the MTA at time t_{2n}. The nth hydrophone is located at $\tilde{r}_{n_T}(t) = [(r_{nx_T} + V_T t), 0]^{\tau}$. It is assumed that the MTA

moves along the X-axis; from the above geometry we have

$$C^2(t_{2n} - t_1)^2 = r_{y_s}^2(t_1) + [r_{x_s}(t_1) - r_{n_T}(t_{2n})]^2. \tag{8}$$

It is important to note here that the above equation includes the travel time of the signal and the movement of the array during this time, which is required by the signal to travel the distance separating the source and the nth hydrophone of the MTA. From Eq. (8) the time t_{2n} can be determined. The next step is to define the signal $S_n(t)$ received at the nth hydrophone. A model for the $S_n(t)$ is derived by using the results of t_{2n} from Eq. (8) and has the form

$$S_n(t) = A \times s[t(1 - \alpha - n\gamma) - T_a + n\Delta], \tag{9}$$

where the parameters $(\alpha, \gamma, T_a, \Delta)$ are defined by

$$\alpha = \frac{r_{x_s}}{X}\frac{V_{x_s}}{C} + \frac{r_{y_s}}{X}\frac{V_{y_s}}{C} - \frac{r_{x_s}}{X}\frac{V_T}{C}, \tag{10.1}$$

$$\gamma = \frac{d}{X}\frac{r_{y_s}}{X}\left(\frac{r_{x_s}}{X}\frac{V_{y_s}}{C} - \frac{r_{y_s}}{X}\frac{V_{x_s}}{C} + \frac{r_{y_s}}{X}\frac{V_T}{C}\right), \tag{10.2}$$

$$T_a = \frac{X}{C}\left(1 - \frac{r_{x_s}}{X}\frac{V_{x_s}}{C} - \frac{r_{y_s}}{X}\frac{V_{y_s}}{C}\right), \tag{10.3}$$

$$\Delta = \frac{d}{C}\frac{r_{x_s}}{X}, \quad X = \left(r_{x_s}^2 + r_{y_s}^2\right)^{1/2}, \quad \cos\beta = \frac{r_{x_s}}{X}, \quad \sin\beta = \frac{r_{x_s}}{X}. \tag{10.4}$$

In the above expressions, there are four fundamental unknowns $(r_{x_s}, r_{y_s}, V_{x_s}, V_{y_s})$ and the known parameters are (d, V_T, C). For a source arbitrarily far away (i.e. $X \to \infty$) we have, $\gamma \to 0$ and $T_a \to \infty$. However, the absolute time delay T_a can be accommodated by simply waiting for the signal to arrive. So Eq. (9) becomes

$$S_n(t) = A \times s[t(1 - \alpha) - T_a + n\Delta], \tag{11}$$

where $\alpha = (V_{x_s} - V_T/C)\cos\beta + V_{y_s}/C \sin\beta$, $\Delta = d/C \cos\beta$ and T_a is arbitrary. The actual received signal $y_n(t)$ by the nth element of the MTA is assumed to be

$$y_n(t) = A \times s[t - D_n(\Theta; t)] + \epsilon_n(t), \tag{12}$$

where $\epsilon_n(t)$ is the gaussian noise which is spatially and temporally white and Θ the vector parameter set. The ML procedure says to minimize energy

$$E_1 = \sum_{n,t}^{N,T} \left[y_n(t) - A \times s\left(t - D_n(\Theta; t)\right)\right]^2, \tag{13}$$

by choice of A and Θ. The symbol $\sum_{n,t}^{N,T} = \sum_{n=0}^{N-1}\sum_{t=0}^{T}$ will be used throughout this report.

For the case where the received signal is a pure tone, we have $\tilde{s}(t) = Be^{-i\phi_s}$, for $t\varepsilon T$. Then Eq. (13) reduces to maximization of

$$E_2 = \left| \int_0^T \left(\sum_{n=0}^{N-1} y_n(t) e^{-i(\omega t + n\phi)} \right) \mathrm{d}t \right|, \tag{14}$$

$$\omega = \tilde{\Omega}_0 \left(1 - \frac{\tilde{V}_s - V_T \cos\tilde{\beta}}{C} \right), \tag{15.1}$$

$$\phi = \frac{d}{C} \tilde{\Omega}_0 \cos\tilde{\beta}. \tag{15.2}$$

Since the envelope of $\tilde{s}(t)$ is independent of t for $t\varepsilon T$ the dependence on $\tilde{\Delta}$ in the above relation has disappeared. From (15), the unknowns $\tilde{\Omega}_0, \tilde{\beta}, \tilde{V}_s$ cannot be uniquely determined. An assumption can be made here that the component of the velocity of the source along its bearing is negligible ($\tilde{V}_s = 0$). This assumption is the same as in Sect. 2. Then the parameters $\tilde{\Omega}_0$ and $\tilde{\beta}$ are uniquely determined from Eq. (15) by searching for the values of ϕ and ω which maximize the term

$$\mathrm{MLE}(\omega, \phi) = \left| \Delta t \sum_{n=0}^{N-1} e^{-in\phi} \left[\sum_{m=1}^{M} y_n(m\Delta t) e^{-im\Delta t\omega} \right] \right|. \tag{16}$$

Equation (16) indicates that the N complex vectors $Y_n(\omega) = \sum_t y_n(t) e^{-i\omega t}$, $n = 1, 2, \ldots, N$ which give the voltage spectrums for the hydrophone time series $y_n(t)$ at ω, are phased together by searching ϕ over $(-\pi, \pi)$ until the largest vector length occurs.

When the single frequency source signal, which is received by the MTA, is considered to be a plane wave, the $y_n(t_i)$ can be expressed by $y_n(t_i) = e^{i(\omega_0 t_i + \phi_0 n)}$ where ω_0, ϕ_0 are the true parameter values. Substituting this expression in (16) and after normalization the relative response of the MLE is

$$P_{\mathrm{MLE}} = \left| \frac{\sin(((\omega - \omega_0)/2)T)}{T(\omega - \omega_0)/2} \frac{\sin(((\phi - \phi_0)/2)N)}{N(\phi - \phi_0)/2} \right|. \tag{17}$$

When the MLE estimates (ω, ϕ) are very close to the true values, the sin function can be approximated by ($\sin x \simeq x - 1/6\, x^3$, for $|x| \ll 1$) and Eq. (17) becomes

$$P_{\mathrm{MLE}} \simeq e^{-1/24[(\omega-\omega_0)^2 T^2 + (\phi-\phi_0)^2 (N^2-1)]}. \tag{18}$$

In order to investigate the resolution capabilities of the MLE, it is assumed that $\tilde{\Omega}_0 = \Omega_0$. Then $\phi - \phi_0 = (\Omega_0/C)\, \mathrm{d}(\cos\tilde{\beta} - \cos\beta)$, and $\omega - \omega_0 = (\Omega_0/C)\, V_T(\cos\tilde{\beta} - \cos\beta)$. Substituting the above in (18) yields

$$P_{\mathrm{MLE}} \simeq e^{-(1/24)[(\Omega_0^2/C^2)(\cos\tilde{\beta} - \cos\beta)^2 [d^2(N^2-1) + V_T^2 T^2]]}. \tag{19}$$

From the above expression, the effective length of the aperture is found to be $L = [d^2(N^2-1) + V_T^2 T^2]^{1/2}$. When $|\cos\tilde{\beta} - \cos\beta| = (\lambda_0/2)/L$ we have from (19), $P_{\text{MLE}} = e^{-\pi^2/24} = 0.66$. This result indicates that the angular resolution of the MTA at a center frequency Ω_0 with wavelength λ_0 and for T seconds observation period is λ_0/L. The effective length of the extended aperture of the MTA is now $L = [d^2(N^2-1) + V_T^2 T^2]^{1/2}$.

Equation (16) is used in this study as an MLE technique when a signal is considered as being a tone, and estimates of $(\tilde{\Omega}_0, \tilde{\beta})$ are provided from Eq. (15). Estimates of ω and ϕ are determined when Eq. (16) reaches the global maximum by a two dimensional search over the above parameters.

3.3. THRESHOLD EFFECT

The performance in bearing estimation of the ETAM algorithm and the MLE can be determined by comparing the $\sigma^2_{\tilde{\beta}_{\text{ETAM}}}(V_T)$, $\sigma^2_{\tilde{\beta}_{\text{MLE}}}(V_T)$ of the above bearing estimates with the CRLBs derived in Sect. 2. For each estimator it is well known that there is a range of SNR in which the variance of the estimates rises very rapidly as SNR decreases. This effect is called the 'threshold of an estimator' and determines the range of the SNR of the received signals for which the parameter estimates can be accepted.

Computer simulation examples have been used to derive estimates of the variance of bearings for the MLE and the ETAM algorithm. For the case of one source, Fig. 7a gives the estimates of $\sigma^2_{\tilde{\beta}_{\text{ETAM}}}(V_T)$, $\sigma^2_{\tilde{\beta}_{\text{MLE}}}(V_T)$ as a function of the SNR and these are compared with the corresponding CRLBs, which are shown by the solid line in this figure. The above results indicate that for both techniques (ETAM, MLE), the $\sigma^2_{\tilde{\beta}_{\text{ETAM}}}(V_T)$, $\sigma^2_{\tilde{\beta}_{\text{MLE}}}(V_T)$ estimates agree with the CRLBs in the range $(0, \infty)$ dB of SNR at the hydrophone. In the range $(-5, 0)$ dB the above estimates start to deviate from the expected ones and this range determines the threshold effect which is the same for both techniques.

The computer simulation example considered for the derivation of the results of Fig. 7a included a towed array having 4 hydrophones, moving with 5 kn towed array and the observation period was 14.5 s. During the above observation period, the extended aperture of the 4-hydrophone MTA was equivalent to a 20-hydrophone fully populated stationary array. The above parameters have been chosen to agree with those of one set of experiments described in Sect. 4.

Presented in the next Fig. 7b are the results of $\sigma^2_{\tilde{\beta}_{\text{ETAM}}}(V_T)$ in comparison with the CRLBs for the case of a 32-hydrophone MTA moving with 5 kn speed and for 80 s observation period. Here again the threshold effect for the ETAM algorithm is 0 dB SNR at the hydrophone. In this figure, results for $\sigma^2_{\tilde{\beta}_{\text{MLE}}}(V_T)$ have not been obtained

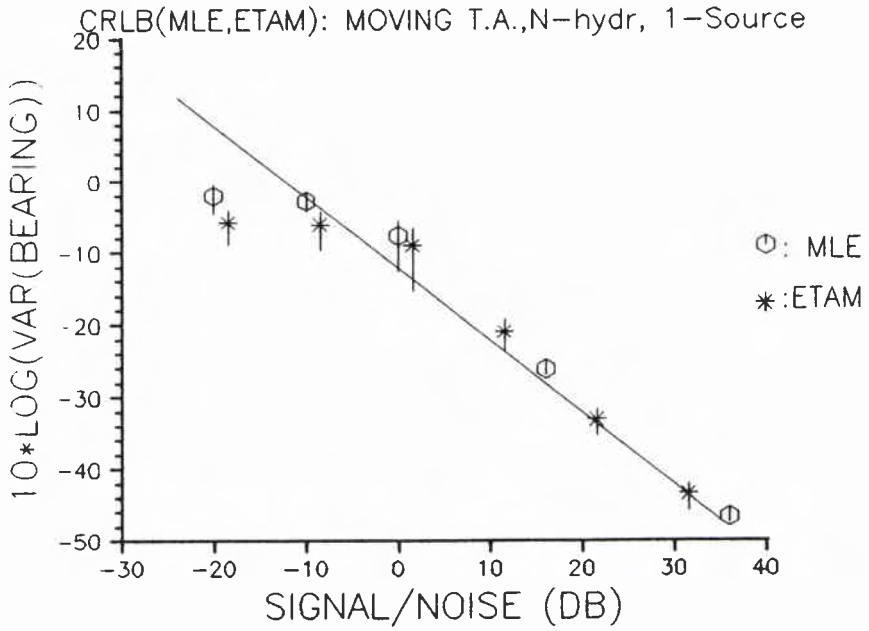

Fig. 7a. Performance in bearing estimation of the ETAM algorithm and the MLE in comparison with the CRLB estimates for the case when one source is known to exist. Results for $\sigma^2_{\hat{\beta}_{\mathrm{ETAM}}}(V_T)$ and $\sigma^2_{\hat{\beta}_{\mathrm{MLE}}}(V_T)$ have been derived from numerical simulation examples and are plotted as a function of the SNR at the hydrophone. The solid line gives the CRLB estimates for $\sigma^2_{\beta_1}(V_T)$ as a function of the SNR for the case of one source and having as unknowns the parameters $(A_1, \Omega_1, \beta_1, \Phi_1)$. In the numerical simulation examples for ETAM and MLE the case of an MTA with 4-hydrophones was considered having $d = 1.96$ m spacing, speed $V_T = 2.5$ m/s and $T = 14.5$ s observation period.

since the MLE technique for this example required very large memory space and very long CPU time.

For the case of two sources, Fig. 8 shows the angular resolution performance of the ETAM algorithm in comparison with the CRLB estimates, which are the same as in Fig. 5. The estimated parameters $\sigma^2_{\hat{\beta}_{\mathrm{ETAM}}}(V_T)$, $\sigma^2_{\beta_{\mathrm{CRLB}}}(V_T)$ have been normalized by $\sigma^2_{\beta_1}$ given by Eq. (4) and are plotted as a function of the angular separation of the two sources. The parameters for the simulation example considered in the above figure include a 32-hydrophone MTA moving with 5 kn and with observation period being 183 s. The extended aperture of the 32-hydrophone MTA is equivalent to a 256-hydrophone fully populated stationary array. In the results of the above figure, there are two different set of examples with total SNR at the hydrophone of 12.8

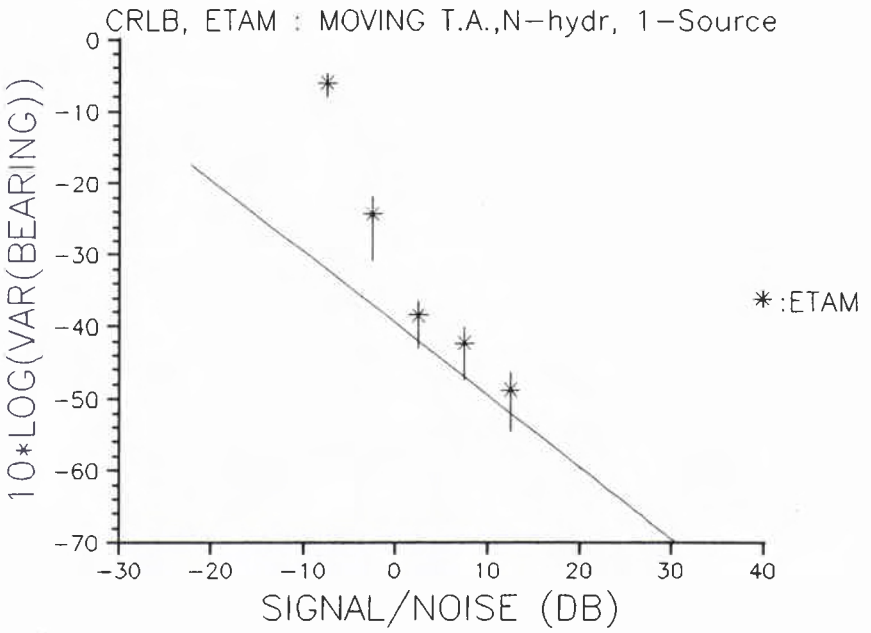

Fig. 7b. Performance in bearing estimation of the ETAM algorithm in comparison with the CRLB estimates for the case when one source is known to exist. Results for $\sigma^2_{\hat{\beta}_{\mathrm{ETAM}}}(V_T)$ have been derived from numerical simulation examples and are plotted as a function of the SNR at the hydrophone. The solid line gives the CRLB estimates for $\sigma^2_{\hat{\beta}_1}(V_T)$ as a function of the SNR for the case of one source and having as unknowns the parameters $(A_1,\ \Omega_1,\ \beta_1,\ \Phi_1)$. In the numerical simulation examples for ETAM the case of an MTA with 32-hydrophones was considered having $d = 1.96$ m spacing, speed $V_T = 2.5$ m/s and $T = 80$ s observation period.

and 2.8 dB, respectively. Since the total SNR is for both sources, the value of the SNR for each source, and for each one of the above two cases, is 6.8 and -3.2 dB, respectively. The above results show that at 3 dB total SNR at the hydrophone level, the $\sigma^2_{\hat{\beta}_{\mathrm{ETAM}}}(V_T)$ estimates have started to deviate from the CRLBs indicating that the threshold of this technique is in the range of 0 dB SNR.

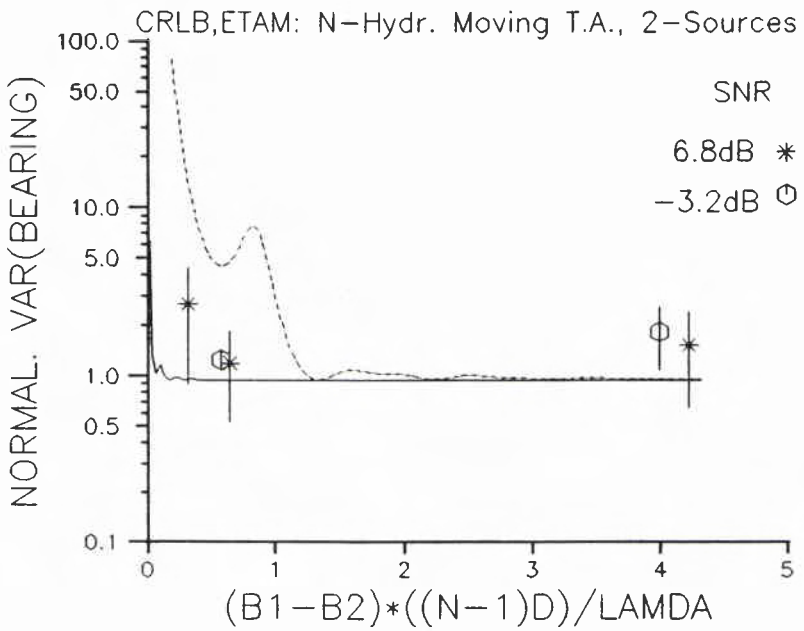

Fig. 8. Angular resolution performance of the ETAM algorithm in comparison with the CRLB estimates for the case when two sources are known to exist. Results for $\sigma^2_{\beta_{\mathrm{ETAM}}}(V_T)$ and $\sigma^2_{\beta_{\mathrm{CRLB}}}(V_T)$ have been normalized by $\sigma^2_{\beta_0}$ given by Eq. (4) and are plotted as a function of the angular separation of the two sources. The estimates of $\sigma^2_{\beta_{\mathrm{ETAM}}}(V_T)$ have been derived from numerical simulation examples. In the CRLB estimates for $\sigma^2_{\beta_{k=1,2}}(V_T)$ unknowns are the parameters of the two sources $(A_k,\ \Omega_k,\ \beta_k,\ \Phi_k)$, $k = 1, 2$. Curve 1 (dashed line) gives the $\sigma^2_{\beta_{\mathrm{CRLB}}}(V_T)$ for $T = 1.0$ s and curve 2 (solid line) gives $\sigma^2_{\beta_{\mathrm{CRLB}}}(V_T)$ for $T = 183$ s. In the numerical simulation examples for ETAM the case of an MTA with 32-hydrophones was considered having $d = 0.98$ m spacing, speed $V_T = 2.5$ m/s and $T = 183$ s observation period. The SNR at the hydrophone for the estimates of $\sigma^2_{\beta_{\mathrm{ETAM}}}(V_T)$ is shown by the different symbols. In the two examples considered here the values of SNR for each source were 6.8 and −3.2 dB, respectively.

4

Experiments

There are two kinds of experimental setups which have been used in this study in order to examine the performance of the ETAM algorithm and the MLE on real data. The measurement procedure in these experiments included two research vessels. The first one was used to tow a receiving array with 64 hydrophones spaced at 0.98 m. The second vessel was towing a projector which transmitted CW signals at various depths and frequencies. In the first experimental set up, the vessel with the projector was stationary. In the second set up, this vessel was moving along a straight-line course which was parallel or with 45° heading relative to the other tow vessel with the receiving array. The data acquisition and control system included amplification of the hydrophone signals, bandpass filtering, digitization and continuous recording on a high-performance digital recorder for off-line processing of the time series. The results reported in this section are divided into two parts. The first part presents the measurements when the source was stationary, and the second part describes the measurements when the source was moving.

4.1. STATIONARY SOURCE

In this set of experiments, the receiving array and the projector were at 100 m depth. The projector transmitted a series of CW pulses of 16 s duration at 333 Hz. The signals were received by an array of 32 hydrophones spaced at 1.96 m. The water depth was 2500 m and the range between the projector and the receiver was 45 km. The towship was moving along a straight-line course with 5 kn. For this set of measurements there is a separate study about the spatial and temporal stability of low-frequency acoustic signals [16]. The conclusion from this study says that in the received signal the frequency is very stable and the phase has a continuous drift of 3π rad during the 16 s time interval.

The curve 1 in Fig. 9a presents the beamforming from the first set of 20 hydrophones of the receiving towed array. The SNR in the hydrophone time series was very high (50 dB). In this curve the estimated bearing of the source agrees with the expected value. Shown in curve 2 of this figure are the bearing estimates using the ETAM algorithm on the first 4 hydrophones of the receiving array and for 14.5 s observation period. Results from the application of the MLE on the same set of data as in curve 2 of Fig. 9a are given in Fig. 10. The extended physical aperture in the results

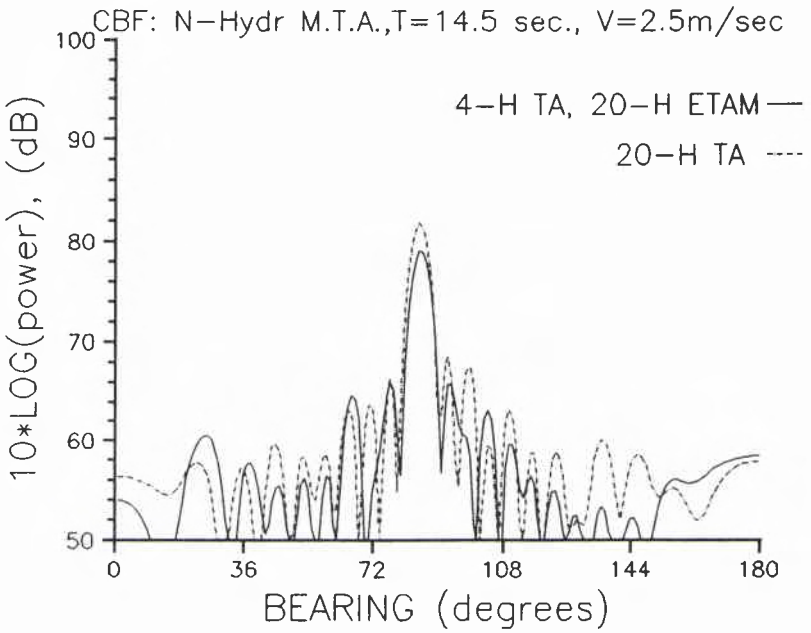

Fig. 9a. Bearing estimates of an active source from real data received by an MTA moving with 5 kn. The range between the projector and the receiver was 45 km, the water depth was 2500 m and the depth of the receiver and the projector was 100 m. Curve 1 (dashed line) gives bearing estimates by beamforming frequency domain data from 20-hydrophones at $f = 333$ Hz. Curve 2 (solid line) gives bearing estimates by beamforming extended aperture data using the ETAM from 4-hydrophone time series with $T = 14.5$ s observation period and at $f = 333$ Hz. The extended aperture is equivalent to a 20-hydrophone fully populated array.

of Fig. 10 and of curve 2 of Fig. 9a is equivalent to a 20-hydrophone fully populated array and the bearing estimates shown by curves 1, 2 and Fig. 10 are identical.

Results from the application of the synthetic aperture concept, which has been presented in Subsect. 3.1, on the same set of data of curve 2 in Fig. 9a are given by curve 2 of Fig. 9b. Curve 1 in this figure gives for comparison the results from beamforming the first set of 20 hydrophones of the receiving array. This curve is the same as curve 1 in Fig. 9a. Apparently the poor performance of the synthetic aperture technique in comparison with the performance of the two methods presented here is due to the reported [16] phase variations in the received signal. It has been shown here by the results of Figs. 9 and 10, and by another numerical study [5] that when

attempts are made to extend the physical aperture of an MTA, these phase variations can be compensated properly by the ETAM algorithm and the MLE.

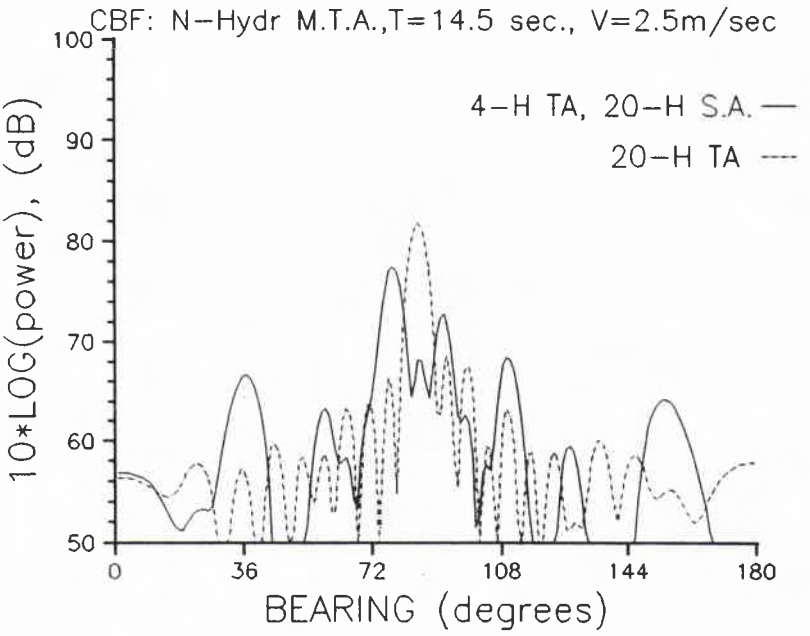

Fig. 9b. Shown by curve 1 (dashed line) are the bearing estimates by beamforming frequency domain data from 20-hydrophones at $f =$ 333 Hz. The above set of data are the same as in the curve 1 of Fig. 9a. Curve 2 (solid line) gives bearing estimates by beamforming 20-hydrophone *synthetic aperture* data, which have been derived from 4-hydrophone time series using the *synthetic aperture technique*. The selected frequency for beamforming was the same as in the results of the above curve 1.

4.2. MOVING SOURCE

Measurements were performed in shallow water with 300–500 m depth. The sea-state was 5. The vessel towing the projector was moving along a straight-line course which was parallel to the heading of the vessel towing the hydrophone array. This parallel course had been followed when the projector was active. The speed for both vessels was 5 kn and their separation range was about 8 km. The receiving array had 64 hydrophones spaced at 0.98 m and the projector was transmitting continuously a CW signal having two tones at 550 and 750 Hz. The depth for

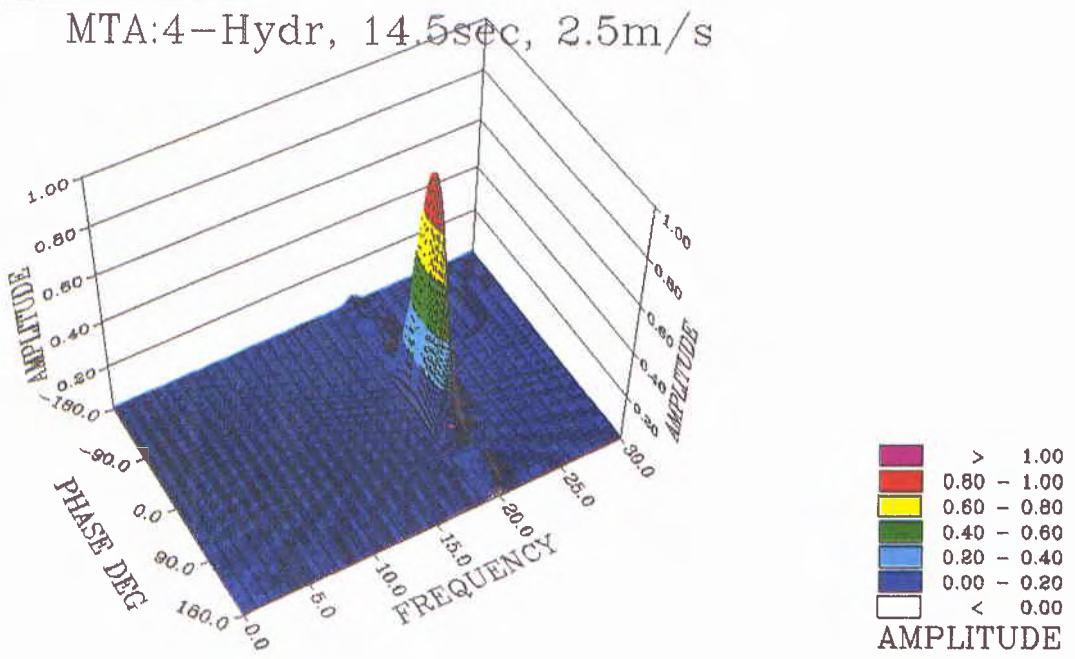

Fig. 10. Results from the application of the MLE on the same set of 4-hydrophone time series as in the curves 2 of Figs. 9a and b. $T = 14.5$ s is the observation period and the 2-D search has provided estimates for the frequency and the bearing of the active source, which are the same with those of the curves 1 and 2 of Fig. 9a.

both the receiving array and the projector was about 100 m. The data acquisition and control system provided continuous recording of the received signal. Shown by the schematic diagram in Fig. 11 is the general arrangement for the above set of experiments.

Pure tone CW signal In the set of measurements with the source moving, the physical aperture was extended by 8 or 16 times using the ETAM algorithm. The MLE technique has not been applied in this set of measurements because of the very large memory and long CPU execution time requirements. Shown in Fig. 12 is the power spectrum of one of the hydrophone time series, which has been processed with a numerical bandpass filter centered at 750 Hz. The received tone at 750 Hz has a very high SNR. The results from beamforming the 64 hydrophones of the receiving array are given by curve 1 of Fig. 13. The frequency bin considered in this beamforming was at 750 Hz. As expected, the results from this curve of the bearing estimates for the projector are in agreement with the expected values. Presented by curve 2 in the same Fig. 13 are the bearing estimates for the first 8 hydrophones of the receiving array and for 23 s observation period. The extended physical aperture

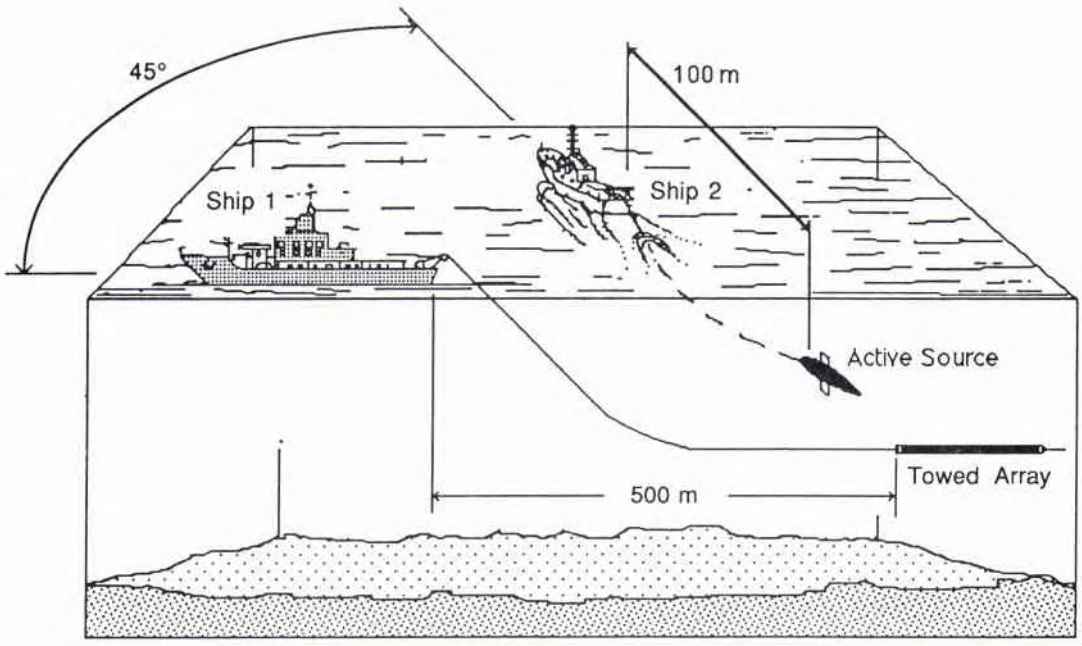

Fig. 11. General arrangement for the set of experiments with the moving source. The depth of the moving towed array and the projector was 100 m and their separation range was 8 km. The water depth was 300–500 m. The speed for the two ships was 5 kn.

for the measurements in curve 2 is equivalent to a 64-hydrophone fully populated array and the results in curves 1 and 2 are the same, indicating that the ETAM algorithm is efficient to extend the physical aperture of a small array by 8 times.

Results from the application of the ETAM on 32 hydrophones of the receiving array and for 185 s observation period are given by curve 2 in Fig. 14. The extended physical aperture in this case is equivalent to a 512-hydrophone fully populated array. In the same figure, curve 1 gives for comparison the results for the actual 64 hydrophone array which are the same as those in curve 1 of Fig. 13. It is very interesting to note here that the improvement in the bearing estimates from the synthesized 512 hydrophones in comparison with the one of the 64-hydrophone array is higher by 12 dB. This gain would have been the same if a fully populated 512 hydrophone array had been used to derive the same measurements.

Results for the same set of data in time and space domain as those in Figs. 13 and 14 but at a different frequency, which is the other tone at 550 Hz, are given in Figs. 15a,b. Curve 1 in these figures gives the bearing estimates from the 64-hydrophone actual array. Curve 2 in Fig. 15a gives the bearing obtained from a synthesized 64 element array, which was derived from 8 hydrophones of the receiving

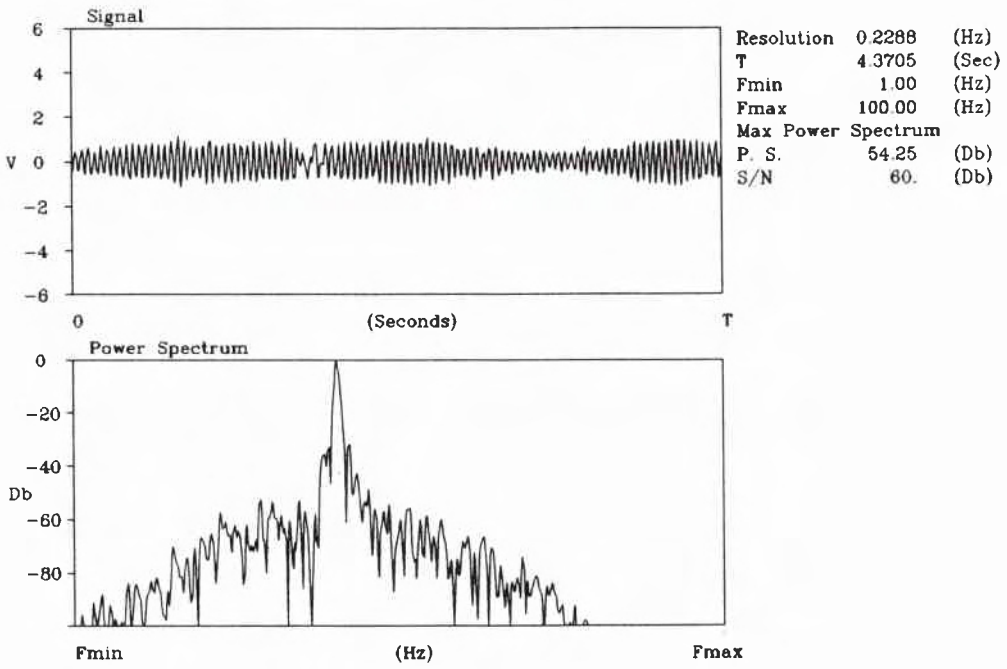

Fig. 12. Shown in the upper part is the received signal by the hydrophones of the towed array. The digitized time series have been filtered and decimated to include in this case only one tone which was 750 Hz. In the lower part the power spectrum of the above decimated time series is shown. The received tone, which is clearly shown in the above spectrum, corresponds to the 750 Hz transmitted tone from the projector.

array. Curve 2 in Fig. 15b gives the results for a 512-hydrophone extended aperture derived from a 32-hydrophone physical array. All the bearing estimates in Figs. 15a,b are in agreement with those of Figs. 13 and 14 since they refer to the same source in time and space domain.

Broadband signal A major concern in the theoretical development of the ETAM algorithm [5] and the MLE technique [12] was the assumption about the received signal being a pure tone. This assumption raised concerns about the usefulness of the ETAM algorithm for cases with broadband signals. In order to confront this issue, a new set of experimental measurements was carried out with the projector silent. In this case the radiated noise of the vessel towing the projector was considered to be the broadband signal, which was received by the hydrophone array. This vessel followed a straight-line course with 45° heading relative to the other vessel towing the array. This relative heading between the broadband source and the receiver created a non-zero radial velocity for the source, which is a violation of the assumption in

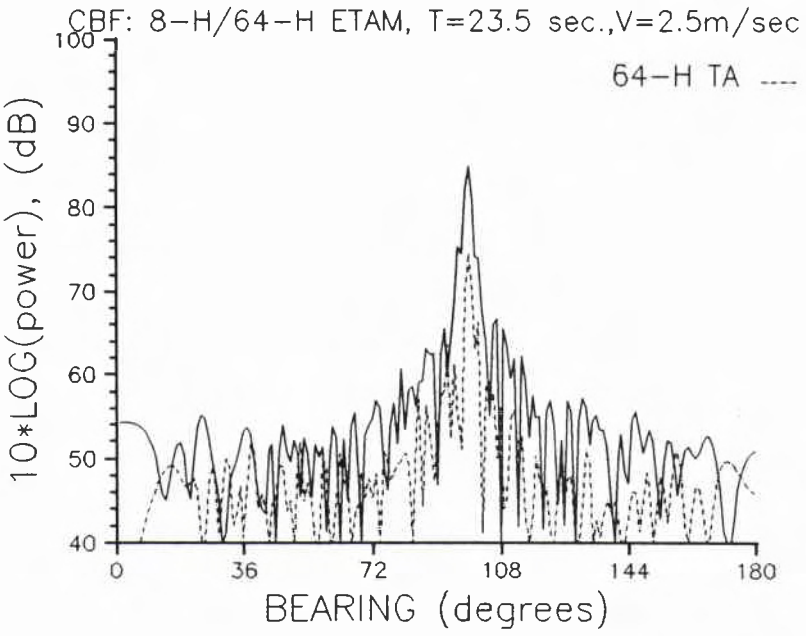

Fig. 13. Shown by curve 2 (solid line) are the bearing estimates of the source by beamforming 64 extended towed-array space samples, which have been derived from 8-hydrophone time series with $T = 23.5$ s observation period using the ETAM algorithm. For comparison curve 1 (dashed line) gives the bearing estimates by beamforming 64-hydrophone space samples of the fully populated array. The frequency selected for beamforming was derived from the peak shown in the power spectrum of Fig. 12.

Sect. 2 of this report, which assumed zero radial velocity for the source. In the following analysis of this new set of measurements, both the above complications about the broadband signal and the non-zero radial velocity would be very good tests for the robustness of the ETAM algorithm.

Presented in Fig. 16 is a typical record of the hydrophone time series, which includes the broadband signal and its power spectrum. The beamforming of the 64 hydrophone time series at a frequency bin near 750 Hz is given by curve 1 of Fig. 17. The bearing estimate in this curve is in agreement with the expected bearing of the vessel towing the silent projector. The beamforming of the above 64 space samples at any other frequency in the range 700–750 Hz would provide similar bearing estimates indicating that the received signal is broadband and originates from the above vessel. Shown by curve 2 in the same Fig. 17 is the bearing estimate from 64 synthesized hydrophones derived from 8 hydrophones of the receiving array

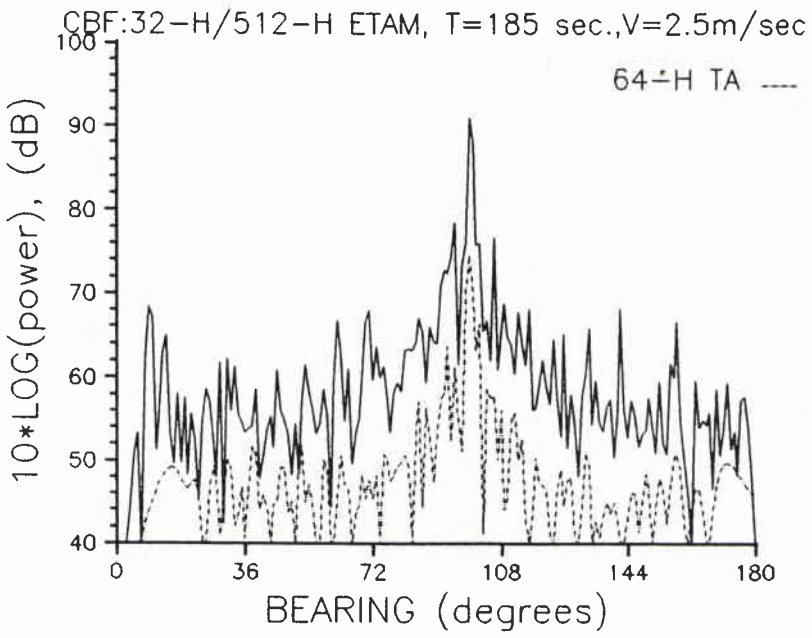

Fig. 14. Shown by curve 2 (solid line) are the bearing estimates of the source by beamforming 512 extended towed-array hydrophone measurements,which have been derived from 32-hydrophone towed-array time series with $T = 185$ s observation period by using the ETAM algorithm. For comparison the bearing estimates from a 64-hydrophone fully populated array are given by the curve 1 (dashed line) which has the same set of results as the curve 1 of Fig. 13.

using the ETAM algorithm. The bearing results in the above two curves are nearly identical.

In Fig. 18 the bearing estimate of the above vessel is given by curve 2, which is obtained from the beamforming of 512 synthesized hydrophones derived from a segment of 32 hydrophones of the receiving array. For comparison, the bearing estimate from the actual 64-hydrophone array is shown by curve 1 in the same figure. The frequency bin used for beamforming, for all the cases presented in Figs. 17 and 18, was the same and is shown by the arrow in Fig. 16, which gives the power spectrum of the received signal.

The power levels of the bearing estimate in Figs. 17 and 18 indicate that the extended physical aperture using the ETAM algorithm has exploited the available space and time coherence of the underwater environment. If there are no phase variations in the received signal, then the synthetic aperture technique would also

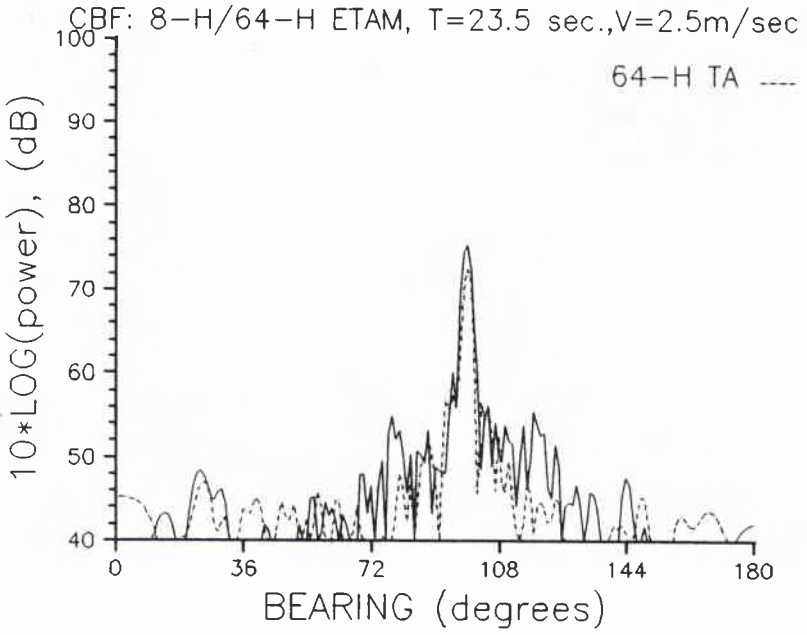

Fig. 15a. Bearing estimates of the source from 64-extended towed-array measurements using the ETAM algorithm. The arrangement of this set of results is the same as in Fig. 13 with the only difference that the frequency selected for beamforming was the other received tone, which was 550 Hz. The above set of measurements correspond to the same space position and moment as those in Fig. 13 and the bearing estimates in both the above figures are the same.

coherently synthesize an extended aperture. For this set of data there are reported measurements [16], which show that the phase variations in the received signal for this particular underwater environment have a continuous drift of about 8π rad during 16 s of observation period. It is expected, therefore, that the synthetic aperture technique would not provide coherent synthesis of an extended aperture for this set of data. This is demonstrated by the results of Fig. 19. Shown by curve 2 in this figure is the beamforming of 64 synthesized hydrophones derived from 8 hydrophones of the receiving array by using the synthetic aperture technique. For comparison, the beamforming of the actual 64 hydrophones is shown by curve 1 in the same figure. The incoherent synthesis of the 64 hydrophones in this case is shown by the power levels in the bearing estimates between curves 1 and 2 in Fig. 19. This incoherent synthesis is also shown by the failure to determine the bearing of the source in curve 2 of Fig. 19.

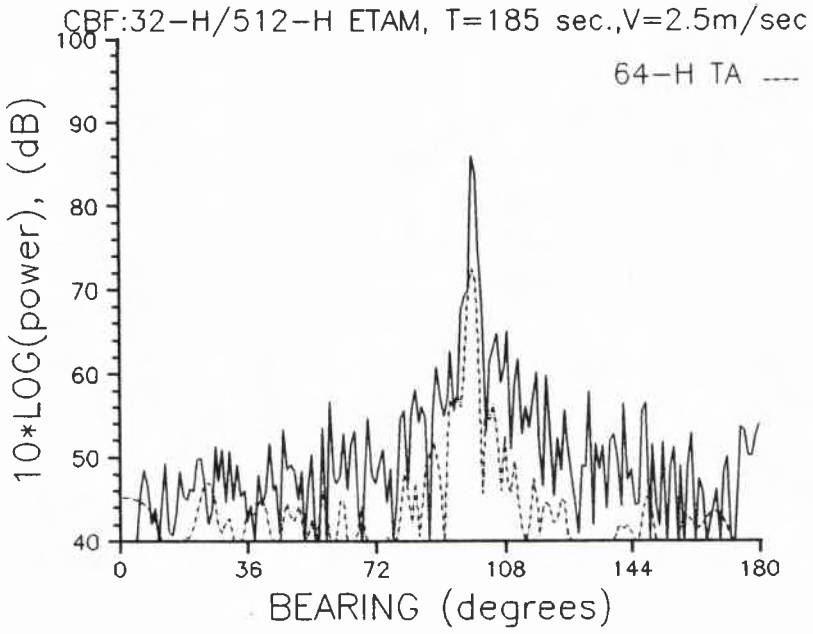

Fig. 15b. Bearing estimates of the source from 512-extended towed-array measurements using the ETAM algorithm. The arrangement of this set of results is the same as in Fig. 14 with the only difference that the frequency selected for beamforming was the other received tone, which was 550 Hz. The above set of measurements correspond to the same space position and moment as those in Fig. 14 and the bearing estimates in both the above figures are the same.

Broadband signal with very low SNR Although the estimated threshold SNR of the ETAM in Subsect. 3.3 is in the range of 0 dB, the experimental measurements, which have been used here to examine the performance of this algorithm, had very high SNR. Therefore, a question to be addressed here is about the performance of the above algorithm in real data with low SNR. Since the above experimental set up does not provide data of this kind directly, an attempt is made here to get measurements with low SNR from the existing data.

The main difference in the power spectra shown in Figs. 11 and 16 is that in Fig. 16 the spectrum of the towship's radiated noise is given while in Fig. 11 the CW signal frequency at 750 Hz and the spectrum of the towship's noise are present. The power spectrum of the towship's radiated noise in Fig. 11, however, has very low SNR because the CW signal is very strong. In this case the analog-to-digital converter (ADC) uses most of the available 12 bit resolution to describe the strong CW signal

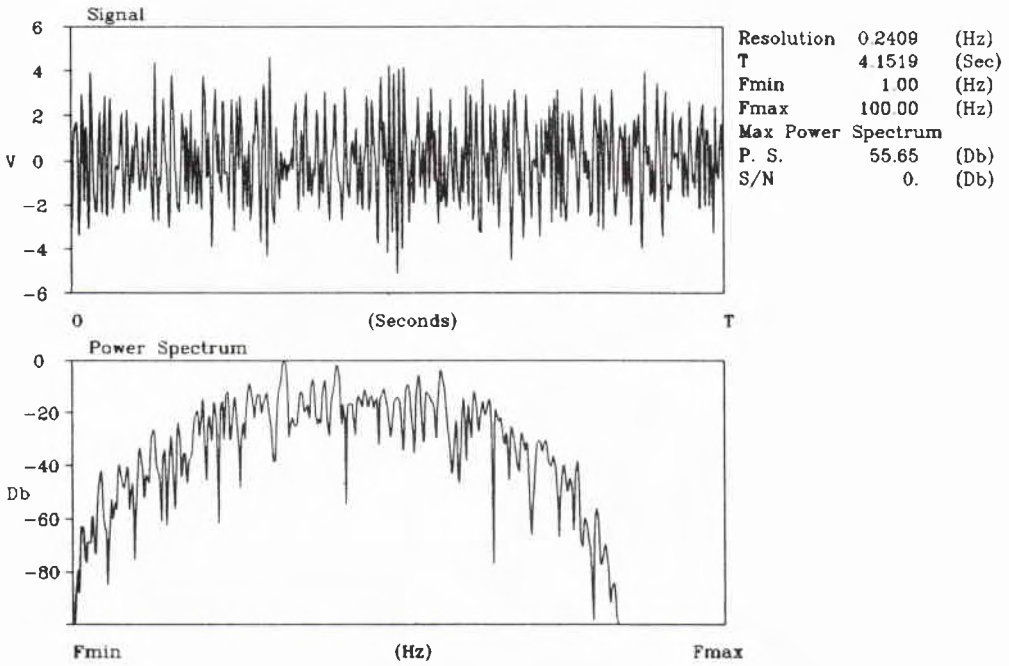

Fig. 16. Shown in the upper part is the received signal by the hydrophones of the towed array. The digitized time series have been filtered and decimated to include the frequency range 700–800 Hz of the broadband spectrum of the radiated noise from the ship towing the silent projector. In the lower part the power spectrum of the above decimated time series is shown. The arrows indicate the selected frequencies for beamforming, which give the same bearing estimates corresponding to the bearing of the above vessel.

and only 2 or 3 bits are used for the towship's radiated noise. Therefore, any frequency with very low SNR from the spectrum shown in Fig. 11, except the one at 750 Hz, is related to the broadband noise of the projector's towship.

Presented in Fig. 20a is the bearing estimates from beamforming the 64-hydrophone physical array at 731 Hz. The bearing shown by this curve is related to the projector's towship and is the same as in curve 1 of Fig. 13. As expected, results from beamforming a 512-hydrophone synthesized array, which is derived by the ETAM from a 32-hydrophone segment of the actual array, are better than those of curve 1 and are given by the solid curve in Fig. 20a. There are other frequency lines in the broadband spectrum of Fig. 12, which provide very poor bearing estimates by beamforming the 64-hydrophone physical array and this is shown by curve 1 of Fig. 20b giving bearing estimates from 64-hydrophone physical array at 736 Hz. For this frequency line, however, the results from beamforming 512-hydrophone ex-

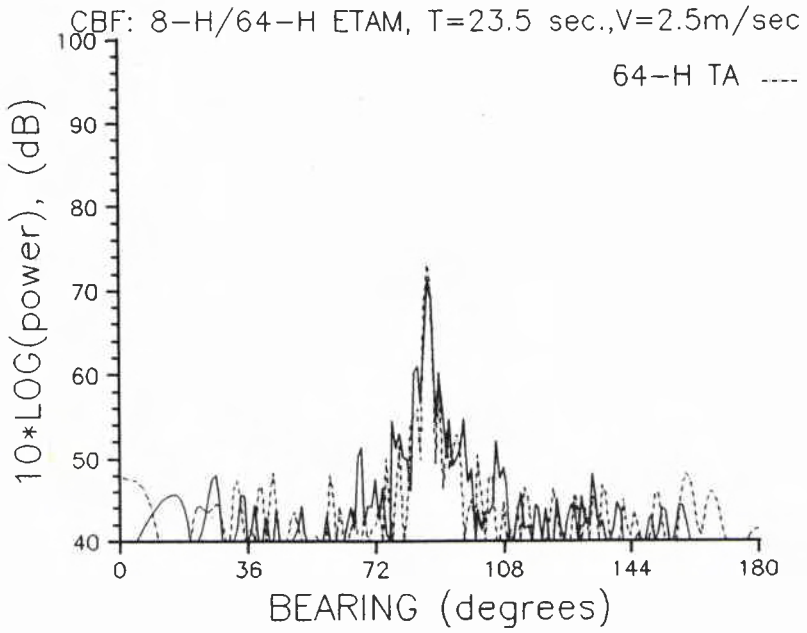

Fig. 17. Bearing estimates for the vessel towing the silent projector from 64-extended towed-array measurements using the ETAM algorithm. The arrangement of this set of results is the same as in Fig. 13 with the only difference that the frequency selected for beamforming was the 750 Hz from the broadband radiated signal. The above set of measurements correspond to a different space position and moment with those of Fig. 13. The bearing estimates derived from the 64-hydrophone extended towed-array measurements are nearly identical with those derived from the 64-hydrophone fully populated array indicating the efficiency of the ETAM algorithm to extend successfully 8 times the physical aperture of an MTA by exploiting the available space coherence.

tended aperture give much better estimates than for the 64-hydrophone array; this is shown in Fig. 20b. This of course does not always happen. In particular, the bearing estimate shown by curve 1 of Fig. 21 is the result of beamforming the 64-hydrophone physical array at 742 Hz. The above bearing estimate is better than the one provided by the 512 hydrophone extended aperture and is shown here by curve 2 of Fig. 21. It is believed that this effect is due to the time instability and coherence of some of the frequency lines of the broadband signal and its investigation is beyond the scope of this report.

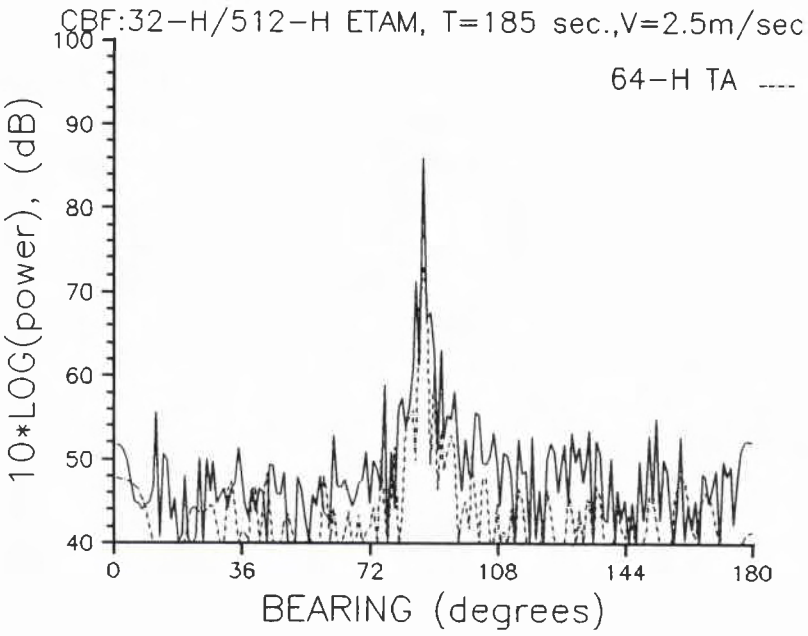

Fig. 18. Bearing estimates for the vessel towing the silent projector from 512-extended towed-array measurements using the ETAM algorithm. The arrangement of this set of results is the same as in Fig. 14 with the only difference that the frequency selected for beamforming was the 750 Hz from the broadband radiated signal. The above set of measurements correspond to a different space position and moment with those of Fig. 14. The bearing estimates derived from the 512-hydrophone extended towed-array measurements have better resolution and higher power in the beamforming results than the ones derived from the 64-hydrophone fully populated array indicating the efficiency of the ETAM algorithm to extend successfully 16 times the physical aperture of an MTA by exploiting the available space coherence.

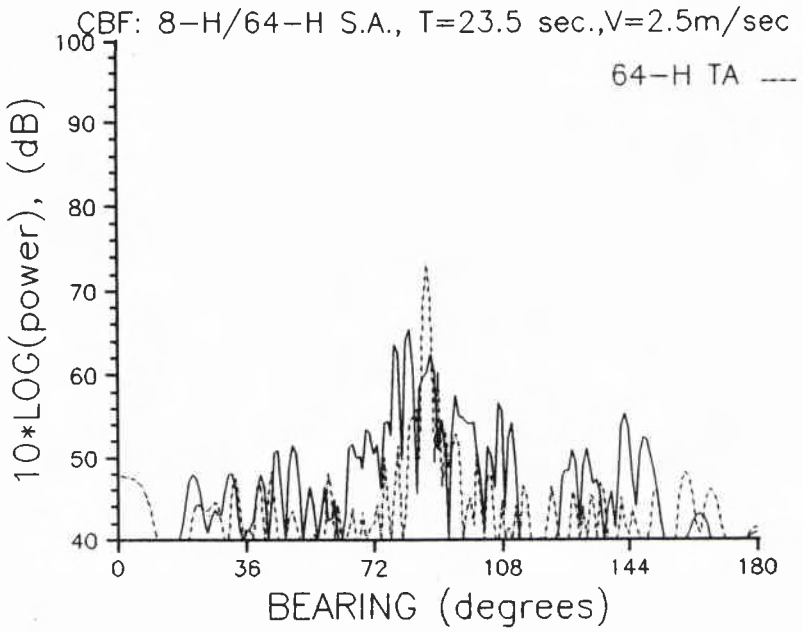

Fig. 19. Shown by curve 1 (dashed line) are the bearing estimates by beamforming the 64-hydrophone space samples of the fully populated array. The results of curve 1 are the same with those of the curve 1 in Figs. 17 and 18. Curve 2 (solid line) gives the bearing estimates by beamforming 64-hydrophones *synthetic aperture* data, which have been synthesized from a segment of 8-hydrophones of the actual receiving array by using the *synthetic aperture technique*. A direct comparison between the above results with those of Fig. 17 indicate the advantages of the ETAM algorithm over the *synthetic aperture technique* to fully exploit the available space coherence of the media in order to extend the physical aperture of an array.

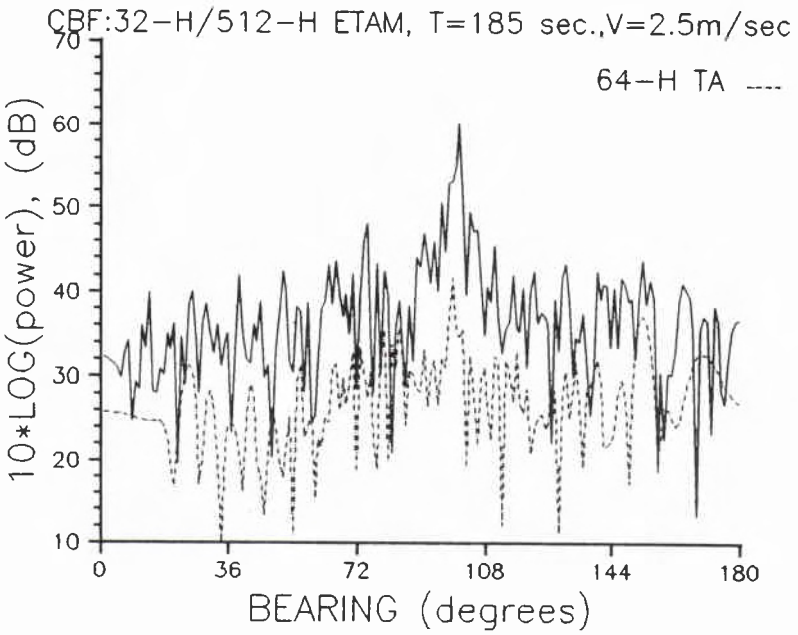

Fig. 20a. Bearing estimates for the vessel towing the active projector from very low SNR 512-extended towed-array measurements using the ETAM algorithm. The arrangement of this set of results is the same as in Fig. 14 with the only difference that the frequency selected for beamforming was the 731 Hz from the broadband radiated signal, which has 60 dB less power level than the tone shown in Fig. 12. The above set of measurements correspond to the same space position and moment with those of Fig. 14. The bearing estimates derived from the 512-hydrophone extended towed-array measurements have better resolution and higher power in the beamforming results than the ones derived from the 64-hydrophones fully populated array, which are shown by the dashed line. The above bearing estimates agree with the expected bearing of the tow vessel of the active projector.

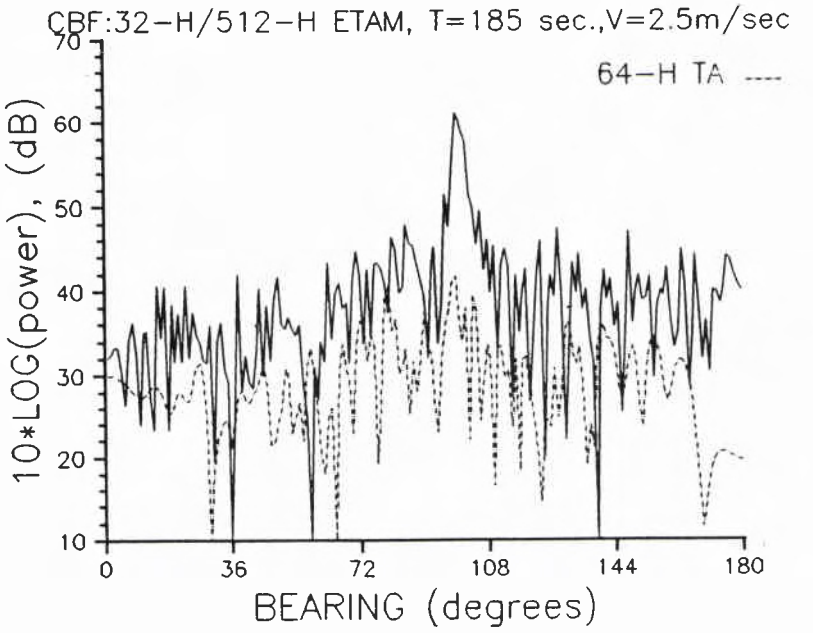

Fig. 20b. Bearing estimates for the vessel towing the active projector from very low SNR 512-extended towed-array measurements using the ETAM algorithm. The arrangement of this set of results is the same as in Fig. 14 with the only difference that the frequency selected for beamforming was the 736 Hz from the broadband radiated signal, which has 60 dB less power level than the tone shown in Fig. 12. The above set of measurements correspond to the same space position and moment with those of Fig. 14. The bearing estimates derived from the 512-hydrophone extended towed-array measurements have better resolution and higher power in the beamforming results than the ones derived from the 64-hydrophones fully populated array, which are shown by the dashed line. The above bearing estimates agree with the expected bearing of the tow vessel of the active projector.

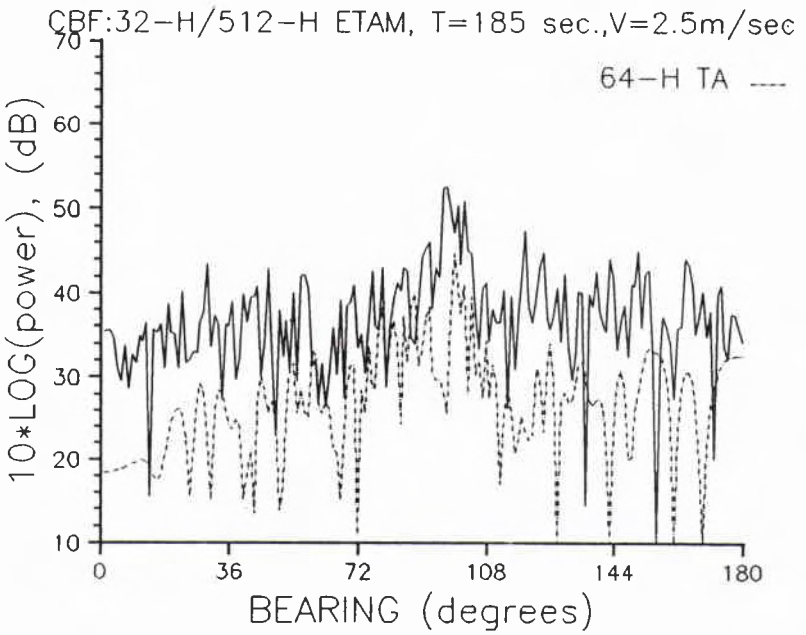

Fig. 21. Bearing estimates for the vessel towing the active projector from very low SNR 512-extended towed-array measurements using the ETAM algorithm. The arrangement of this set of results is the same as in Fig. 14 with the only difference that the frequency selected for beamforming was the 742 Hz from the broadband radiated signal, which has 60 dB less power level than the tone shown in Fig. 12. The above set of measurements correspond to the same space position and moment with those of Fig. 14. The bearing estimates derived from the 512-hydrophone extended towed-array measurements are very poor in this case and the same remarks are for the bearings derived from the 64-hydrophone fully populated array, which are shown by the dashed line. The above poor performance indicates that the selected frequency line to apply the ETAM and to beamform the hydrophone space samples of the physical array did not have have enough information related to the tow ship of the active projector.

5 Conclusions

The theoretical investigation presented in this report, based on the information inequality, has shown that the amount of information inherent in a moving array in comparison with a stationary one is best exploited when the frequency of the source is known. For the cases when the frequencies and the bearings of two or more sources are unknown, the additional information provided by a moving array over a stationary array is expressed as a high increase in angular resolution only when long observation periods of the order of few minutes are used. It has been shown [4], however, that these long observation periods do not necessarily provide a practical equivalent increase in detection performance. In other words the MTA has exploited the amount of information of a long observation period in order to increase the angular resolution by extending the physical aperture of the array, while for a stationary array, that would improve the detection performance.

An MLE technique and the ETAM algorithm have achieved the estimated CRLBs, derived for the problem of a moving array, and their threshold effect is in the range of 0 dB SNR at the hydrophone. An important conclusion drawn here is that the ETAM algorithm yields ML estimates and has comparable performance with an MLE technique. This is expected since the ETAM is based on cross-correlation via FFT and this is in agreement with the conclusion of another study [11] that the FFT for a single-tone parameter estimation is an ML estimator.

Results from applications of the MLE and the ETAM algorithm on real data with pure tone CW signals have shown great consistency between the bearing estimates obtained by extending the physical aperture of an array with those of an equivalent fully populated array. Extensive applications of the ETAM algorithm on real data, which consisted of a pure tone CW signal and a broad band radiated noise from a ship, revealed the following. This algorithm extends successfully the physical aperture of a 32-hydrophone MTA to a synthesized 512-hydrophone array during 185 s of observation time. The performance of the ETAM is very robust since it provides a 16 times extension of a physical aperture of an MTA for a very low SNR broadband signal and for a moving source with non-zero radial velocity. There are questions, however, whether this robust performance of the ETAM still holds for fast moving sources.

It is also equally important to note here that the results from beamforming the extended towed-array measurements for all the different cases shown in Figs. 13–

15, 17, 18 and 20 provide bearing estimates, which are consistent not only with the expected values of the bearings but they also have the correct power level differences. What is meant here by correct differences in power levels of bearing estimates is related to the difference in power levels of the frequency lines shown in Fig. 12 and to the number of hydrophones of arrays which are used for beamforming.

If there is no coherence in the synthesized measurements of an extended aperture then there is always failure to determine bearing estimates and the corresponding power levels are small. This picture of incoherence is shown in Figs. 19 and 21 and their results yield a good criterion to appreciate the effectiveness of the ETAM to extend coherently very long apertures; this is shown by the results of Figs. 13–15, 17, 18 and 20.

It is apparent from the above theoretical and experimental results that there is coherence in the underwater environment which is sufficient to extend the physical aperture of an MTA by more than 16 times. The above results, however, bring another requirement which is related to a new definition and experimental measurement of parameters for coherence when they are intended to be used to extend the physical aperture of an MTA.

References

[1] Williams, R.E. Creating an acoustic synthetic aperture in the ocean. *Journal of the Acoustical Society of America*, **60**, 1976: 60–73.

[2] Broek, H.W. Temporal and spatial fluctuations in single-path underwater acoustic wave fronts, I: Transmission from the first convergence zone at 43 n.mi range. *Journal of the Acoustical Society of America*, **72**, 1982: 1527–1532.

[3] Koenigs, P.D., Herstein, P.D. and Browning, D.G. Further study of the space and time stability of a narrowband acoustic signal in the ocean: short range results. *Journal of the Acoustical Society of America*, **70**, 1981: S16:H3.

[4] Owsley, N.L. Discrete space-time synthetic aperture formation, NUSC TM 861013. New London CT, Naval Underwater Systems Center, 1985.

[5] Stergiopoulos, S. and Sullivan, E.J. Extended towed-array processor by overlapped correlator, SACLANTCEN SM-214. La Spezia, Italy, SACLANT Undersea Research Centre, 1988.

[6] Autrey, S.W. Passive synthetic arrays. *Journal of the Acoustical Society of America*, **84**, 1988: 592–598.

[7] Schulteiss, P.M. and Ianniello, J.P. Optimum range and bearing estimation with randomly perturbed arrays. *Journal of the Acoustical Society of America*, **68**, 1980: 167–173.

[8] Zimmer, W.M.X. High-resolution beamforming techniques, performance analysis, SACLANTCEN SR-104. La Spezia, Italy, SACLANT ASW Research Centre, 1986. [AD A 179 060]

[9] Sklar, J.R. and Schweppe, F.C. On the angular resolution of multiple targets. *Proceedings of the IEEE*, **52**, 1964: 1044–1045.

[10] Kumaresan, R. and Tufts, W.D. Estimating the parameters of exponentially damped sinusoids and pole-zero modeling in noise. *IEEE Transactions on Acoustics, Speech and Signal Processing*, **30**, 1982: 833–840.

[11] Rife, D.C. and Boorstyn, R.R. Single-tone parameter estimation from discrete-time observations. *IEEE Transactions on Information Theory*, **20**, 1974: 591–598.

[12] Nuttall, A.H. Unpublished notes and private communication. New London CT, Naval Underwater Systems Center, November 1988.

[13] Van Trees, H.L. Detection, Estimation and Modulation Theory. New York, NY, Wiley, 1968.

[14] Brennan, L.E. Angular accuracy of a phased array radar. *IRE Transactions on Antennas and Propagation*, **9**, 1961: 268–275.

[15] Pusone, E.G. and Lloyd, L.J. Synthetic-aperture sonar: performance analysis of beamforming and system design. SACLANTCEN SR-91. La Spezia, Italy, SACLANT ASW Research Centre, 1985. [AD A 170 252]

[16] Enoch, P.J. Some effects of spatial and temporal stability on low-frequency sonar signals in the Mediterranean sea. Report in preparation, SACLANT Undersea Research Centre, La Spezia, Italy, 1988.

Appendix A

CRLB analytical derivations

The model which has been considered in this study to describe the observations for an N-element equally spaced hydrophone array has been presented in Sect. 2. This model is the following

$$y_n(t_i) = x_n(\Theta, t_i) + \epsilon_{n,i}(0, \sigma_N), \tag{A.1}$$

with

$$x_n(\Theta, t_i) = \sum_{k=1}^{2} A_k \cos\left[\omega_k \left(t_i + \frac{d(n-1)}{C}\cos\beta_k\right) + \Phi_k\right], \tag{A.2}$$

where $\omega_k = \Omega_k(1 - (V_k - V_T \cos\beta_k)/C)$ is the received frequency which is defined to include the doppler shift and Ω_k the frequency of the stationary field. The notation used here and the definition of the related parameters is the same as in Sect. 2. Since the noise $\epsilon_{n,i}(0, \sigma_N)$ associated with the observations in Eq. (A.1) is assumed to be gaussian, the probability density governing these observations is

$$P(Y|\Theta) = \frac{1}{\sqrt{2\pi\sigma^2}} \exp\left(-\frac{[y_n(t_i) - x_n(\Theta, t_i)]^2}{2\sigma_N^2}\right). \tag{A.3}$$

The observations given by the vector $Y = [y_1(t_i), y_2(t_i), \ldots, y_N(t_i)]^\tau$, $i = 1, 2, \ldots, M$ assume M independent time samples for each of the N independent space samples which are described by the model in Eq. (A.2). The vector of the model parameters is $\Theta = [A_k, \Omega_k, \beta_k, \Phi_k]^\tau$, $k = 1, 2$.

Since the time and space samples are independent, we have

$$P(Y|\Theta) = \prod_{n=1}^{N}\left[\prod_{i=1}^{M} p\left(y_n(t_i)|\Theta\right)\right], \tag{A.4}$$

where

$$P(Y|\Theta) = \prod_{n=1}^{N}\left[\prod_{i=1}^{M}\left(\frac{1}{\sqrt{2\pi\sigma_N^2}} \exp\left(-\frac{[y_n(t_i) - x_n(\Theta, t_i)]^2}{2\sigma_N^2}\right)\right)\right], \tag{A.5}$$

and

$$\ln[P(Y|\Theta)] = -\frac{MN}{2}\ln(2\pi\sigma_N^2) - \frac{1}{2\sigma_N^2}\sum_{n=1}^{N}\sum_{i=1}^{M}[y_n(t_i) - x_n(\Theta, t_i)]^2. \tag{A.6}$$

Let $\sigma^2_{\theta_i}$ denote the variance of an unbiased estimate of an unknown parameter θ_i in the vector Θ. The Cramer–Rao [13] bound states that the best unbiased estimate $\tilde{\Theta}$ of the parameter vector Θ has the covariance matrix

$$\mathrm{cov}\tilde{\Theta} \geq J(\Theta)^{-1}, \tag{A.7}$$

where J is the Fisher information matrix whose elements are

$$J_{ij} = -E\left[\frac{\partial^2 \ln P(Y|\Theta)}{\partial\theta_i \partial\theta_j}\right], \tag{A.8}$$

$E[\ldots]$ denotes the expectation operator and $P(Y|\Theta)$, given by Eq. (A.4), is the probability density governing the observations.

The variance $\sigma^2_{\theta_i}$ of the unbiased estimates $\tilde{\Theta}$ has a lower bound called the CRLB which is given by the diagonal elements of Eq. (A.7). This CRLB is used as a standard of performance and provides a good measure for the performance of a signal processing algorithm which gives unbiased estimates $\tilde{\Theta}$ for the parameter vector Θ.

The analytical derivation of the elements of the Fisher information matrix follows from Eq. (A.6):

$$\frac{\partial \ln[P(Y|\Theta)]}{\partial\theta_i} = \frac{1}{\sigma_N^2}\sum_{n=1}^{N}\sum_{i=1}^{M}[y_n(t_i) - x_n(\Theta,t_i)]\frac{\partial x_n(\Theta,t_i)}{\partial\theta_i}, \tag{A.9}$$

$$\frac{\partial^2 \ln[P(Y|\Theta)]}{\partial\theta_i^2} = \frac{1}{\sigma_N^2}\sum_{n=1}^{N}\sum_{i=1}^{M}\left([y_n(t_i) - x_n(\Theta,t_i)]\frac{\partial^2 x_n(\Theta,t_i)}{\partial\theta_i^2} - \left[\frac{\partial x_n(\Theta,t_i)}{\partial\theta_i}\right]^2\right). \tag{A.10}$$

Since $E[y_n(t_i) - x_n(\Theta,t_i)] = 0$, the J_{ij} element of Eq. (A.8) is derived from Eq. (A.10):

$$J_{ij} = -E\left(\frac{\partial^2 \ln[P(Y|\Theta)]}{\partial\theta_i\partial\theta_j}\right) = \frac{1}{\sigma_N^2}\sum_{n=1}^{N}\sum_{i=1}^{M}\left[\frac{\partial x_n(\Theta,t_i)}{\partial\theta_i}\frac{\partial x_n(\Theta,t_i)}{\partial\theta_j}\right]. \tag{A.11}$$

The terms $\partial x_n(\Theta,t_i)/\partial\theta_i$ in the above relation are derived based on the model (A.2). One very good approximation of the above model is

$$x_n(\Theta,t_i) = \sum_{k=1}^{2} A_k \cos\left[\Omega_k\left(1 + \frac{V_T\cos\beta_k}{C}\right)t_i + \Omega_k\left(\frac{d(n-1)}{C}\cos\beta_k\right) + \Phi_k\right], \tag{A.12}$$

where the radial velocity of the source V_k and the term $(V_T d(n-1)/C^2)\cos^2\beta_k$ have been neglected since they are considered negligible. Then for the kth source the terms $\partial x_n(\Theta,t_i)/\partial\theta_i$ are given by

$$\frac{\partial x_n(\Theta,t_i)}{\partial A_k} = \cos(\Psi_k), \tag{A.13}$$

$$\frac{\partial x_n(\Theta,t_i)}{\partial \Omega_k} = -A_k\left[\left(1+\frac{V_T\cos\beta_k}{C}\right)t_i + \frac{d(n-1)}{C}\cos\beta_k\right]\sin(\Psi_k), \tag{A.14}$$

$$\frac{\partial x_n(\Theta,t_i)}{\partial \beta_k} = A_k\sin\beta_k\Omega_k\left[\frac{V_T t_i + d(n-1)}{C}\right]\sin(\Psi_k), \tag{A.15}$$

$$\frac{\partial x_n(\Theta,t_i)}{\partial \Phi_k} = -A_k\sin(\Psi_k), \tag{A.16}$$

where $\Psi_k = \Omega_k[(1+V_T\cos\beta_k/C)t_i + d(n-1)\cos\beta_k/C] + \Phi_k$.

Substituting the above Eqs. (A.13)–(A.16) into (A.11), the J_{ij} terms of the Fisher information matrix are derived. The double summation $\sum_{n=1}^{N}\sum_{i=1}^{M}$ in the above terms was approximated by $\sum_{n=1}^{N}[1/\Delta t\int_{t=0}^{T}\ldots\,\mathrm{d}t]$ where $T = M\Delta t$. It is considered appropriate to reference the integrals and the summations which have been used for the above derivations:

$$\int t\cos(at+\Phi)\,\mathrm{d}t = \frac{\cos(at+\Phi)}{a^2} + \frac{t\sin(at+\Phi)}{a}, \tag{A.17}$$

$$\int t^2\cos(at+\Phi)\,\mathrm{d}t = \frac{2t}{a^2}\cos(at+\Phi) + \left(\frac{t^2}{a} - \frac{2}{a^3}\right)\sin(at+\Phi), \tag{A.18}$$

$$\sum_{n=0}^{N-1}\cos(\Phi+ny) = \cos\left(\Phi+\frac{N-1}{2}y\right)\sin\frac{Ny}{2}\operatorname{cosec}\frac{y}{2}, \tag{A.19}$$

$$\sum_{n=1}^{N-1} n\cos(\Phi+ny) = \frac{N}{2\sin(y/2)}\left[\sin\left(\frac{2N-1}{2}y+\Phi\right) - \sin\Phi\right] - \frac{1}{4\sin^2(y/2)}[\cos(Ny+\Phi)-\cos\Phi]. \tag{A.20}$$

As an example the term $J_{\beta\beta}$ will be evaluated for the case when one source is known to exist and the unknown parameter is the bearing β. From Eqs. (A.11) and (A.15) we have

$$J_{\beta\beta} = \frac{(A_1\Omega_1\sin\beta_1)^2}{\Delta t(C\sigma_N)^2}\sum_{n=1}^{N}\left(\int_0^T[V_T t + d(n-1)]^2\sin^2[\Psi_1(t)]\,\mathrm{d}t\right), \tag{A.21}$$

$$J_{\beta\beta} = \frac{(A_1\Omega_1\sin\beta_1)^2}{2\Delta t(C\sigma_N)^2}\sum_{n=1}^{N}\left(\int_0^T[V_T t + d(n-1)]^2(1-\cos[2\Psi_1(t)])\,\mathrm{d}t\right), \tag{A.22}$$

Initial Distribution for SR-154

Ministries of Defence	
JSPHQ Belgium	2
DND Canada	10
CHOD Denmark	8
MOD France	8
MOD Germany	15
MOD Greece	11
MOD Italy	10
MOD Netherlands	12
CHOD Norway	10
MOD Portugal	5
MOD Spain	2
MOD Turkey	5
MOD UK	20
SECDEF US	60
NATO Authorities	
Defence Planning Committee	3
NAMILCOM	2
SACLANT	3
SACLANTREPEUR	1
CINCWESTLANT/ COMOCEANLANT	1
COMSTRIKFLTANT	1
CINCIBERLANT	1
CINCEASTLANT	1
COMSUBACLANT	1
COMMAIREASTLANT	1
SACEUR	2
CINCNORTH	1
CINCSOUTH	1
COMNAVSOUTH	1
COMSTRIKFORSOUTH	1
COMEDCENT	1
COMMARAIRMED	1
CINCHAN	3
SCNR for SACLANTCEN	
SCNR Belgium	1
SCNR Canada	1
SCNR Denmark	1
SCNR Germany	1
SCNR Greece	1
SCNR Italy	1
SCNR Netherlands	1
SCNR Norway	1
SCNR Portugal	1
SCNR Turkey	1
SCNR UK	1
SCNR US	2
SECGEN Rep. SCNR	1
NAMILCOM Rep. SCNR	1
National Liaison Officers	
NLO Canada	1
NLO Denmark	1
NLO Germany	1
NLO Italy	1
NLO UK	1
NLO US	1
NLR to SACLANT	
NLR Belgium	1
NLR Canada	1
NLR Denmark	1
NLR Germany	1
NLR Greece	1
NLR Italy	1
NLR Netherlands	1
NLR Norway	1
NLR Portugal	1
NLR Turkey	1
NLR UK	1
Total external distribution	236
SACLANTCEN Library	10
Stock	34
Total number of copies	280